

**UNIVERSITÄT
BAYREUTH**

Bachelor Thesis

Spatio-temporal correlation of turbulence in atmospheric boundary layers

Charlotte Geiger

Submission date: October 12, 2023

Department of Theoretical Physics I,
Prof. Dr. Michael Wilczek

Supervisors: Prof. Dr. Michael Wilczek,
Prof. Dr. Christoph Thomas

Acknowledgement

I would like to express my deepest appreciation to Professor M. Wilczek and Professor C. Thomas, who agreed on working with me together. This thesis would not have been possible without their support.

A very big thanks goes to David, whose help cannot be overestimated. You opened the field of programming to me, with your expertise and patience.

I am very grateful for you Anna and Hannah for being in there together:)

I would also like to thank everybody at the chair for your support and suggestions and the fun coffee and lunch breaks.

Thank you, Marius, for believing and for being there for me.

And of course I would specially thank my family: You have always been there for me and supported me. The “GoGoGos” motivated me a lot!

Contents

1	Abstract	4
2	Zusammenfassung	5
3	Introduction	6
4	Theoretical Part	7
4.1	Taylor's frozen-in-flow hypothesis	7
4.2	The random sweeping decorrelation hypothesis	8
4.3	The Elliptic Model	8
4.4	Literature overview for the application and the usage of the elliptic model	10
5	Experimental Set-Up and Declaration of Data	11
5.1	Description of the field experiment set up and the measured air temperature data .	11
5.2	Wavelet high-pass filtering applied prior to analysis	14
6	Methods	17
6.1	Extraction of parameters U_m and V_m using a maxima determination	17
6.2	Extraction of parameter U_e and V_e by fitting an ellipse to the iso-contour lines of the correlation function	20
7	Results	23
7.1	Characteristic types of iso-contour plots	23
7.2	Results of parameters U_m and V_m using the maxima determination method	25
7.3	Results of the values U_e and V_e extracted by the ellipse fit method	27
8	Discussion	31
9	Conclusion	35
	Selbstständigkeitserklärung	38

1 Abstract

For the statistical analysis and modeling of atmospheric boundary flows it is crucial to evaluate their space-time correlations. Significant space-time correlations require high spatially- and temporally-resolved data, which however are difficult to measure in field experiments. Therefore, there is an urge to estimate the correlations using easier accessible one-point measured data. The elliptic model derived by He and Zhang [1] states that iso-correlation lines are elliptic shaped, of which orientation and size is characterised by the mean velocity value U and the sweeping velocity V and can therefore be conducted out of one-point correlations. The model has been proven to provide valid results for several flows and could therefore be a basis for the estimation. But to also prove the model's validity for the atmospheric boundary flow, more studies concerning the application of the elliptic model have to be conducted. In this thesis, I will analyse the shape of the spatio-temporal correlation function $C_{TT}(r, \tau)$ based on temporal fluctuating data conducted with the application of distributed temperature sensing. The calculation of the characteristic parameters U and V will be done using two different methods, the results of which are compared with the measured velocities. My result show that most of the iso-correlation plots show the predicted elliptic lines and that the scale of the measured sweeping V matches the calculates ones. But although the maxima fit method results in a mean velocity that matches the calculated mean velocity, the elliptic fit method results in values that are an order of magnitude smaller, which leads to the conclusion that the elliptic fit method works better for low to zero mean velocity situations. In total, I can conclude that the elliptic model is applicable to the measured data, but has great potential for improvement when applied to higher temporal and spatial resolved data over a larger viewing area.

2 Zusammenfassung

Die Untersuchung der Raum-Zeit-Korrelationen ist für eine statistische Analyse und Modellierung atmosphärischer Grenzströmungen wichtig. Eine aussagekräftige Raum-Zeit-Korrelationen benötigt jedoch räumlich und zeitlich hoch aufgelöste Daten, die in Feldexperimenten schwer zu messen sind. Diese Beschränkung führt zum Versuch, die Korrelationen anhand von leichter zugänglichen Ein-Punkt-Messdaten theoretisch herzuleiten. Ein theoretisches Modell, das diese ein- und zwei-Punkt Korrelationen verbindet, ist das elliptische Modell [1] von He und Zhang. Das Modell besagt, dass Isokorrelationslinien elliptisch geformt sind und daher mit einer Ellipse dargestellt werden kann, deren Orientierung und Größe durch die mittlere Geschwindigkeit U und die "sweeping" Geschwindigkeit V charakterisiert wird. Durch diese Annahme können die Iso-Korrelations Kontour Linien aus Ein-Punkt-Korrelationen hergeleitet werden. Mehrere Experimente haben die Anwendbarkeit des elliptischen Modells für verschiedene Strömungen verifiziert. Um jedoch die Gültigkeit des Modells auch für die atmosphärische Grenzströmung zu analysieren und gegebenenfalls zu bestätigen, müssen weitere Untersuchungen zur Anwendung des elliptischen Modells durchgeführt werden. In dieser Arbeit wird die Form der räumlich-zeitlichen Korrelationsfunktion $C_{TT}(r, \tau)$ anhand von zeitlich fluktuierenden Temperaturdaten analysiert, die mit Hilfe von Temperaturmessungen gewonnen wurden. Die Berechnung der charakteristischen Parameter U und V wird mit zwei verschiedenen Methoden durchgeführt, deren Ergebnisse mit den gemessenen Geschwindigkeiten verglichen werden. Meine Ergebnisse zeigen, dass die meisten Iso-Korrelations Plots die vorhergesagten elliptischen Linien zeigen und dass die Skala der gemessenen Schwingungen V mit den Berechneten übereinstimmt. Aber obwohl die Maxima-Fit-Methode zu einer mittleren Geschwindigkeit führt, die mit der berechneten mittleren Geschwindigkeit übereinstimmt, führt die elliptische Fit-Methode zu Werten, die eine Größenordnung kleiner sind, was zu der Schlussfolgerung führt, dass die elliptische Fit-Methode besser für Situationen mit niedrigen bis keiner mittleren Geschwindigkeiten funktioniert. Das Ergebnis der Arbeit ist, dass das elliptische Modell auf die gemessenen Daten anwendbar ist, jedoch zu teilweise größeren Fehlern führt, was auf die zeitlich und räumliche Auflösung der Daten zurück zu führen ist.

3 Introduction

Atmospheric surface layers rule the turbulent exchange of heat, carbon, energy, and aerosols between the earth's surface and the atmosphere. Their understanding is very important for climate and weather modeling. [2] Due to the boundary of the earth's surface, the fluid velocities in the atmospheric boundary layer vary randomly in space and time, creating a highly chaotic and turbulent flow [3].

This randomness results in a wide range of spatial and temporal scales and constant alteration due to the swirling [4] and prevents a deterministic approach to the problem leading to the necessity of a statistical approach for the analysis of turbulence data [5]. To understand and analyse the factor of change of a variable, a correlation function is often applied. But due to the additional mutual influence of the spatial and temporal variable, a simple one-dimensional correlation function is no longer sufficient, as the connection of both variables is essential.

Therefore in the studies of turbulent flows an approach of 2-dimensional correlation functions, the so called spatio-temporal correlation, has been focused on for decades. Over time, different theories have been developed using this statistical approach for modeling and analyzing turbulent flows [6]. For good and accurate results of the correlation function, it is very important to have access to high-resolution spatio and temporal data [6]. But due to the limitation of field equipment the analysis was long restricted to numerical calculations for example the large eddy simulations. Even though the possibilities of complex numeric data analysis were improved over the last years, the reality of the atmospheric boundary layer consists of many different partly unknown parameters, which cannot be predicted in advance leading to the necessity of field measured data.

But the difficulties of measuring such high-resolution data in the atmospheric boundary layer is leading to a scarcity of experimental measured data. This limitation coupled with the lack of simultaneous measured data, presents a significant limitation for experimental studies and statistical characterization exploring the relationships between space and time [6].

The absence of quantities for two-point-two time measurements, compared to the easier one-point measurements in atmospheric boundary layer, results in a high demand for models that can estimate space-time correlations from one-point measurement data [6]. The most important models for the estimation of space-temporal correlation are the Taylor's frozen-in-motion hypothesis and the elliptic model. To test and verify the applicability of the models for the atmospheric boundary layer in the reality it nevertheless is very important to have real measured data.

For measurements in the atmospheric boundary layer, distributed temperature sensing (DTS) has become a crucial tool for obtaining data with high temporal and spatial resolutions. The fiberoptic system accurately measures small-scale thermal structures in atmospheric flows under various conditions, which can be used to directly estimate the length scales of turbulent motions [7]. The utilization of high temporal and spatial frequency temperature data obtained through DTS and the analysis and the comparison of it with a theoretical model was done by Han and Zhang [6] who analyzed the space-temporal correlation function $C_{TT}(r, \tau)$ and investigated the suitability of the elliptic model in the atmospheric boundary layer and developed a method for estimating the value of $C_{TT}(r, \tau)$ based on this model.

The intention of this thesis is to analyse, whether the experimental set up of 2011 of the team of Christoph Thomas can also be used for a comparison of the measured spatio-temporal correlation and the elliptic model. This paper is organized as follows:

The first section introduces the elliptic model, its motivation and theoretical background and gives detailed explanations for important keywords related to the model. The second section describes the set up of the field experiment of Christoph Thomas conducted in the USA 2011 [7]. In addition the regime classification and its characteristic parameters are explained and applied on the measured data and the limitations and its justifications for the used data is pointed out. A limitation to the stable and labile regimes was applied due to the resolution of the data, which is further explained in the section. The wavelet filter function, used as a bandpass filter for separating low and high frequency data is characterised and its characteristic separation parameter analysed. After that, the two methods of calculating the two characteristic velocity parameters of the elliptic, the mean velocity U and the random sweeping velocity V , is presented in detail. In the forth section, the results are specified and in the further sections, the possibilities and limitations of the two approaches discussed and the conclusions about it are drawn.

4 Theoretical Part

As motivated in the introduction, the focus of this paper lies upon the analysis of atmospheric boundary layer, which represents the lowest air layer of the atmosphere with direct connection to the ground[8]. As the name implies, it represents a boundary situation for air flow, which is leading to turbulent motion [9].

Turbulence is defined as a highly chaotic flow characterized by random fluctuations [3]. This randomness prevents a deterministic approach to the problem leading to the necessity of a statistical approach for the analysis of turbulence data [5].

A turbulent flow can be explained by breaking down the flow into clusters of flow particle packages that have the same characteristics as velocity or energy content. These characteristics of these so-called eddies break down in size and energy content in the dissipation process, which can be determined by statistical methods, in the spectral or real space. A lot of spectral analysis has been made, leading to theory of the “energy cascade” by Kolmogorov [10], which states that energy of large scale eddies is transferred during the dissipation process to smaller and smaller structures in the characteristic decay of $-5/3$. Besides the dissipation process, there is no

statistical interaction between two scales of motion[11].

This leads for the spatial spectrum to:

$$E(k) = \epsilon^{2/3} k^{-5/3} f(k/k_c) \quad (1)$$

The following analysis is based on the assumption of statistically steady, homogeneous, isotropic and incompressible turbulence. In this paper I will focus on the analysis of turbulence in real space. One of the possible approach to do so, is via the correlation function, which analyses the degree of similarity between signals [5].

Besides the auto-correlation, which shows the self-similarity of a single variable, there is also the possibility of connecting signals from two spatially separated measuring positions over time [12]. The so-called spatio-temporal correlation takes the time lag τ in connection to the time t and the spatial shift r to the spatial position x into account, which leads to the relation

$$C(r, \tau) = \langle u_1(x, t) u_2(x + r, t + \tau) \rangle \quad (2)$$

where $\langle \rangle$ marks averaging and u_1 and u_2 represent the two different measurement positions [12]. Due to the potential coupling spatial and temporal scales of motion in turbulence, the spatial-temporal correlation has been employed to develop time-accurate turbulence models. But due to the necessity of simplification of the chaotic flow, the usage and calculation of the correlation is based on approximations and assumptions about turbulence movement.

The results of the correlation function applied to measured data of the atmospheric boundary layer show a spatial and temporal decorrelation. This can be explained with two effects. The turbulent eddies are transported with a mean velocity leading to a spatial decorrelation, which is explained theoretically in the frozen-flow-hypothesis by Taylor. In addition to the mean velocity transportation, in a turbulent flow small eddies are advected with a local mean velocity, that varies spatially and temporal in a random manner. This phenomenon of transportation is called sweeping and results in a statistical distribution of time shifts for a specific spatial shift. This phenomenon leading to the temporal decorrelation is theoretically described with the random sweeping hypothesis of Tennekes and Kraichnan [11]. Since the results show a spatial, as well as the temporal decorrelation, one needs a model that includes both. The model that incorporates the Taylor’s frozen-in-flow and the random sweeping hypothesis is the elliptic model elaborated by He and Zhang [1].

Due to the importance of understanding the physical phenomena of frozen in flow and the random sweeping assumptions for the understanding of the elliptic model, I will dedicate a subsection each, before describing the elliptic model in detail. In the end of this section I will give a short overview of research that has been made so far analysing the elliptic model.

4.1 Taylor’s frozen-in-flow hypothesis

Taylor made one of the first approximations for the analysis of turbulent flows. The so-called frozen-in-flow approximation proposes a “derivation of spatial fluctuations from temporal fluctuations in one point” [9]. The approximation is based on the hypothesis, that the eddy characteristics do not vary during advection and that the eddies are all only advected by the mean flow velocity.

This assumption leads to the conclusion, that the characteristics of the eddies can be described by measurements of only one measurement point, as the data about temporal fluctuations include all information about spatial fluctuations [13].

The frozen-in-flow hypothesis only holds “if the velocity of the air stream carrying the eddies is very much greater than the turbulent velocity” [9]. This means, that “the eddy structures have to be moved past a stationary probe in a time smaller than the inherent evolution time of the fluctuations” [14].

As one-point measurements are well measurable, the Taylor’s frozen-in-flow hypothesis states an assumption, that transforms usual accessible temporal data into nontrivial accessible spatial turbulent data. This potential for knowledge gain led to the realization of a lot of studies about the hypothesis, including the analysis of spatial-temporal correlation. Due to the inclusion of all characteristic data values in temporal data, the two-point spatial correlation function can be related to the temporal auto-correlation function of turbulent velocity at a fixed point [13].

For the derivation of this statement, we start with a spatial pattern of turbulent motion that is carried past a fixed point by the convection speed U without any essential changes:

$$u_1(x+r, t+\tau) = u_1(x+r-U\cdot\tau, t). \quad (3)$$

where r is the spatially streamwise separation, and τ is the temporal separation and inserted this equation into the spatio-temporal correlation of streamwise velocity fluctuation 2 leads to the auto-correlation

$$C(r, \tau) = C(r-U\cdot\tau, 0) = c. \quad (4)$$

One can see, that c is a constant, which implies straight iso-correlation contours lines with the gradient of the mean velocity U [1]. But as numerical and experimental studies have shown, “iso-correlation contours in turbulent shear flows are elongated and closed curves with a preference direction” [1]. These result lead to the conclusion that the frozen-in-flow hypothesis does not describe all physical phenomena of turbulent flows.

4.2 The random sweeping decorrelation hypothesis

The random sweeping decorrelation hypothesis is based on the assumption that small eddies are advected in a turbulent flow with a local mean velocity by large eddies. The local velocity, by which the eddies are transported, varies spatially and temporal randomly in its value, leading to a statistical distribution of time shifts for a specific spatial shift. Tennekes suggests, that the transport of these small scales is related to the energy content of the larger eddies, due to their “direct contribution to the kinetic energy per unit mass of the smaller scales within the Eulerian inertial subrange” [11]. Therefore, “the kinetic energy per unit mass of the larger scales u_i should be considered in the dimensional analysis of the inertial subrange in the Eulerian framework”. Based on this argument, the Eulerian frequency spectra can be described as

$$E_\omega(\omega) = \alpha \langle \epsilon \rangle^{2/3} \langle u_i^2 \rangle^{1/3} \omega^{-5/3} \quad (5)$$

Due to the proportional relation of the kinetic energy per mass to the square of its velocity, we can rewrite the equation into:

$$E_\omega(\omega) = \epsilon^{2/3} V^{2/3} \omega^{-5/3} f(\omega/\omega_c) \quad (6)$$

V represents the sweeping velocity, $f(\omega/\omega_c)$ represents a constant. Similar to the frozen-in-flow hypothesis, this model also has limitations. In the paper [11] by Katul et al., two substantial assumptions of the model were analysed. These assumptions were “(i) the absence of large-scale/inertial subrange interaction, and (ii) the absence of any eddy-motion distortions due to thermal disturbances”. For the atmospheric boundary flow, both assumptions didn’t completely hold, which leads to the conclusion, that the hypothesis does not fully apply for atmospheric boundary flows [11].

4.3 The Elliptic Model

The motivation of the elliptic model is that numerical simulations and experiments lead to elliptic shaped iso-correlation contour lines [1]. An iso-correlation contour line is defined as representing

a specific correlation value $C(r, \tau) = c$. At a particular point, the iso-contour line cuts the spatial shift axis r , which will be defined as point $(r_c, 0)$. This leads us to the connection of

$$C(r, \tau) = c = C(r_c, 0) \quad (7)$$

The reason why the experiments do not show straight lines, is “largely because Taylor’s frozen turbulence hypothesis is only a first-order approximation of iso-correlation contours” [1]. Therefore to receive the elliptic approximation, the elliptic model introduces a higher-order approximation to the iso-correlation contours of the frozen turbulence hypothesis by expanding the correlation function $C(r, \tau)$ about the origin to second order in the Taylor series. For the derivation of the elliptic model we follow the lines of the paper [1] by He and Zhang. The application of the Taylor expansion leads us to the following equation

$$C(r, \tau) = C(0, 0) + \frac{\delta^2 C(0, 0)}{\delta r \delta \tau} r \tau + \frac{1}{2} \left[\frac{\delta^2 C(0, 0)}{\delta r^2} + \frac{\delta^2 C(0, 0)}{\delta \tau^2} \right]. \quad (8)$$

where $\delta_r C(0, 0) = 0$ due to homogeneity and due to stationary $\delta_\tau C(0, 0) = 0$. To receive a relation for r_c , the following substitution are used:

$$U = -\frac{\delta^2 C(0, 0)}{\delta r \delta \tau} \left[\frac{\delta^2 C(0, 0)}{\delta r^2} \right]^{-1} \quad (9)$$

$$V^2 = \frac{\delta^2 C(0, 0)}{\delta \tau^2} \left[\frac{\delta^2 C(0, 0)}{\delta r^2} \right]^{-1} - U^2 \quad (10)$$

and inserting it in the previous equation results in

$$C(r, \tau) = C(r_c, 0) = C(\sqrt{(r - U\tau)^2 + (V\tau)^2}, 0). \quad (11)$$

Therefore the elliptic model states that the iso-contour lines of a spatio-temporal correlation function can be described as ellipses fulfilling the relation

$$r_c^2 = (r - U\tau)^2 + (V\tau)^2. \quad (12)$$

The derivation of the statement of U being the mean velocity and V representing the sweeping velocity was done by He and Zhang and can be found in their paper [1]. In the particular case that V is approximately zero, the equation can be simplified to the equation $r_c^2 = r + U_e \cdot \tau$, which is the same result as the frozen-in-flow hypothesis, and is therefore also leading to straight iso-correlation contour lines. So it becomes obvious that the frozen in flow hypothesis is a borderline case of the elliptic hypothesis [1].

The elliptic model also incorporates the random sweeping hypothesis. To prove this statement, I will transform the elliptic model in Fourier space and compare it with the results of the random decorrelation sweeping hypothesis. The spatial correlation can be written as

$$C(r, 0) = \int dk E(k) \cos kr \quad (13)$$

where E is the spectrum.

The temporal correlation is defined as

$$C(0, \tau) = \int d\omega E_\omega(\omega) \cos(\omega\tau) \quad (14)$$

which can be rewritten to the following equation using the sweeping hypothesis and the elliptic model

$$C(0, \tau) = \int dk E(k) \cos(kV\tau). \quad (15)$$

By using the elliptic model I can write

$$C(r, \tau) = C(r_c, 0) = \int dk E(k) \cos(2\pi k r_c(r, \tau)) = \int dk E(k) \exp[irk \sqrt{(r - U\tau)^2 + (V\tau)^2}] \quad (16)$$

With a change of variables $\omega = Vk$, we obtain $VE_\omega(Vk) = E(k)$. Therefore in the case of the mean velocity U being equal zero, the equation becomes $r^2 + V^2\tau^2 = r_E^2$ resulting in elliptic shaped iso-correlation contour lines with “their preference direction in the horizontal axis” [1]. This leads to the conclusion that the “sweeping hypothesis is implying the same result as the elliptic model up to second order” [1].

Therefore the elliptic model can be used to differentiate between the two different turbulence velocities, the mean velocity at which the eddies are transported, and the sweeping velocity. The latter is “associated with the timescale at which the eddies break apart” [15]. The elliptic model is used in the following analysis as a basis to describe the results of the spatial-temporal correlation of the measured data in the atmospheric boundary layer.

4.4 Literature overview for the application and the usage of the elliptic model

Due to the benefit of the elliptic model of incorporating both, the frozen-in-flow hypothesis and the random sweeping hypothesis, a lot of research has been dedicated to the model. In this section I will list a selection of the research so far that has been conducted using simulations laboratory and field experiments.

- The elliptic model has been applied by He and Zhang to space-time correlations of streamwise velocity fluctuation in turbulent shear flows based on data from direct numerical simulation. The application lead to iso-correlation contour lines that are “like the elliptic curves in alignment with a straight line of the slope U ”, where U is the mean streamwise velocity [1].
- He and Tong have applied the elliptic model to the space-time correlation function in turbulent Rayleigh–Bénard convection. The analysed convective flow “is generated in a confined system between two horizontal plates separated by a distance L and heated from below in the presence of gravity”. The investigation was done at different representative locations in the convection cell leading to results supporting the validity of the elliptic model for the velocity and local temperature fields [16].
- The validity of the elliptic model is also demonstrated by Zhang and Wan using numerical large eddy simulation data representing a turbulent jet flow. The analysis of the space-time correlations $C(r, \tau)$ leads to the conclusion that the calculated elliptical curves match very well the iso-contour lines as well as that the measured mean velocity U and the sweeping velocity V are strongly correlated with the calculated U and V [17].
- Wang et al. [18] showed that the performance of the elliptic model can also be assessed by the data of a turbulent boundary layers flow measured by tomographic time-resolved particle image velocimetry.
- Wilczek and Narita proposed a derivation of an energy model spectrum “in the wave-number–frequency domain including the mean and sweeping velocities” that can be compared with the elliptic model, in real space. Despite the different approaches of the model spectrum and the elliptic model, the model “been shown to be closely related to the recently introduced elliptic model” [19].
- The elliptic model was applied to the longitudinal space–time correlations of temperature fluctuations, that were directly measured in the near-neutral, unstable, and stable atmospheric boundary layer. Additionally to the calculation of the elliptic model based on the measured data, Han and Zhang suggest a possible method for estimating the correlation function $C_{TT}(r, \tau)$ from the elliptic method. As space–time correlations are often restricted to the requirements of high spatially- and temporally-resolved data which is technically difficult to implement, the proposed method could be a promising contribution to the analysis of the atmospheric boundary layer [6].

5 Experimental Set-Up and Declaration of Data

First the setup of the field experiment is described in detail. Then the limitation for filtering the data using specific criteria in this thesis are motivated and applied, resulting in an overview of the used observations for the ensuing analysis. Lastly, the wavelet filtering method, which was applied prior to statistical analysis, is described in detail.

5.1 Description of the field experiment set up and the measured air temperature data

The temperature data were measured with the fiber-optic distributed sensing (FODS, best use [7], or [20]) technology using a fiber-optic cable interrogated by a Distributed Temperature Sensing (DTS) instrument. This technology uses Raman spectra scattering in an optical fiber to measure temperature along its length. The FODS array was installed at the Botany and Plant Pathology laboratory of the Oregon State University, Oregon, USA. Its setup and geometry is described in [21]. Observations were collected between 23 August and 14 October 2011. The geometry of the set up can be described as a quasi-3-dimensional construction consisting of a vertical plane in the north-south direction and three perpendicular vertical planes in the east-west direction [21]. The dimensions of the constructions were 42 m long, 12m wide, and 4.2 m high. The planes are made of wooden structures, which provide a support structure for the measurement fibre. This fibre was spanned in regular spaced vertical strands each consisting of 35 measurement points, equally spaced every 0.1273 m along the fiber. The lateral separation of the vertical strands is 0.255 m, which in total represent 276 vertical profiles. The measured air temperature data were averaged for each spatial point, resulting in a 1 s average every 5.2 s. The whole set-up was oriented with a 6° degree offset to the direct north direction. A visualisation of the field set up can be seen in the figure. A more detailed report of the observation site, experimental setup, and the FODS system can be found in [21] by Zeeman et al.

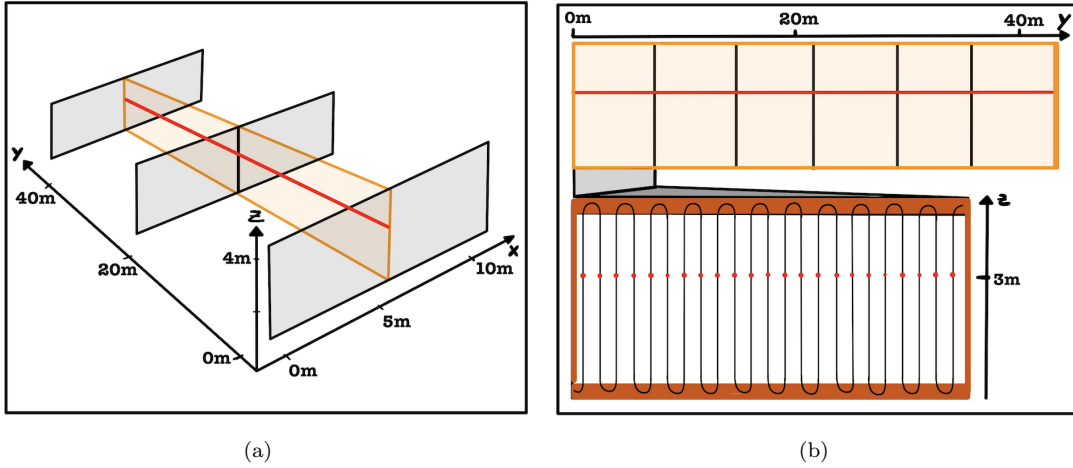


Figure 1: Sketch of the visualization of the field measurement construction.

a) Structure sketch of the quasi-3-dimensional construction. The orange plane represents the middle plane, and the red line represents its height of 3m on which we will focus on in the analysis of this thesis.

b) The front view of the middle plane and a close up to one of the frames including the 23 vertical strands and the measurement points of the height 3m is displayed for better comprehensibility

In addition to the quasi-3-dimensional structure explained before, an ultrasonic anemometer was operated at the height of 3m. The sonic recorded the atmospheric turbulent flow at 20 Hz sampling frequency, and allowed for computing diverse parameters including the direction and speed of the wind mean velocity, the turbulent buoyancy flux, and the friction velocity needed to derive atmospheric stability. Due to the storage of the data in 60min files, I will use these packages in my analysis and will refer to them as data files.

With the parameters that the ultrasonic anemometer provides, one can cluster the data pool into different sections and limit it for reasonable analysis. Four filtering criteria were applied and are listed and justified in the following. The first one is the restriction to the measured data of the long vertical middle plane as it provides the longest continuous measurement series. That can be seen in the figure 1(a). This is important as data for “space-time correlations are restricted to the requirements of highly spatially and temporal-resolved data” [6].

The second requirement is limiting the accepted wind direction. This limitation is done as “direct measurements of $C_{TT}(r, \tau)$ requires that the direction of the optic cable is the same as the direction of the streamwise velocity component (along wind direction)”[6]. But due to the dynamic situation of wind in the Atmospheric boundary there are only few situations of the wind flowing exactly along the long vertical plane compared to the total amount of measured data. Therefore the restriction of the wind direction to less and equal than 15 degree difference to the perpendicular vertical plane along northing was made. The wind that was measured with an angle range of 351° to 21° is a north wind and the wind measured with an angle range of 171° to 201° is a south wind. The sketch of it can be seen in the figure 2, in which the blue lines pictures the maximum of possible angle of the wind permitted in this thesis.

Third, to gain the measurement situation of having an optic cable in the along wind direction, only measurement points at one height of the vertical strands is taken figure 1(b). The height of 3 m above ground was selected matching that of the measurement height of the ultrasonic anemometer for error minimization.

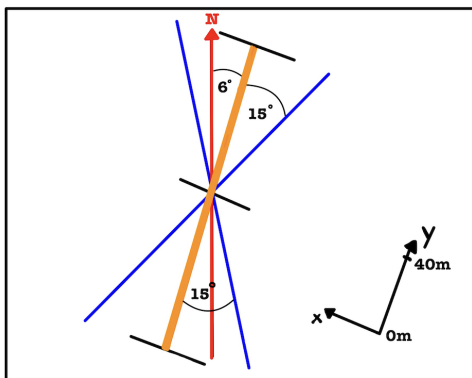


Figure 2: Sketch of permitted wind origin direction including the offset orientation of the quasi-3-dimensional construction towards the northing. The top view of the construction is displayed. The orange line represents its middle plane and the black line its three perpendicular vertical planes. The blue lines pictures the maximum of the wind angle permitted in this thesis. The red line represents the north-south direction, to which the construction is oriented with an offset of 6 degrees.

The last restriction was done using the regime classification, which was applied with the intention of better evaluation of the application of the elliptic model.

There are two parameters that are used for evaluating the stability of the atmospheric boundary layer and classifying the states of the atmospheric surface layer leading to four different regimes: the shear regime, the labile regime, the quiescent regime and the stable (submeso) regime [7]. The first parameter used for the classification is the Monin-Obukhov stability parameter $\zeta = z/L$ in which z is the height, and L is the Obukhov length [6]. The Obukhov length L is defined as [22]

$$L = \frac{\bar{T}u_*^3}{\kappa g(\bar{\omega}T + 0.61\bar{T}\bar{\omega}q)} \quad (17)$$

where κ is the von-Kármán constant, $g = 9.81m/s^{-2}$ is the acceleration due to gravity, and \bar{T} is the mean temperature. The friction velocities u_* , surface sensible heat fluxes H , and surface latent heat fluxes E are calculated using the eddy-covariance method and therefore are

$$u_* = (\overline{uw^2} + \overline{vw^2})^{1/4},$$

$$H = \rho C_p \overline{\omega T},$$

$$E = \rho L_\nu \overline{\omega q},$$

where u, ν is the the streamwise, and ω are the spanwise, respectively the vertical velocity component. q is the specific humidity and the parameter ρ is the air density. The parameter C_p and L_ν are the air specific heat capacity at constant pressure respectively the latent heat of vaporization of water. The kinematic heat flux $\overline{\omega T}$ is calculated by averaging the covariance between the fluctuating vertical velocity component ω and fluctuating temperature T , $\overline{\omega q}$ is calculated by averaging the covariance between the fluctuating vertical velocity component ω and specific humidity q , where the overline represents a temporal average. This definition and further information to the Obukhov length can be found in the paper [22] by Li and Bou-Zeid. The second parameter used for the regime classification is the mean velocity U_{mean} . This parameter for the horizontal wind speed is limited by the resolution of the set up and the height of the measurement points. As the height is 3 m the value of U_{mean} is limited to less or equal 1 ms^{-1} for the analysis of the data measured with the above described construction [7]. This limitations leads to the impossibility of observing the shear flow regime due to its definition of mean wind velocities of higher than 1.6 ms^{-1} . In addition the analysis of the quiescent regime is not done in this thesis, due to the regimes definition of dominating fine-scale turbulent eddies, which can not be dissolved with the spatial and temporal resolution of the measurement.

This leads to the focus on the labile and the stable regime in this thesis. In the following tabular, one can see the parameter values of the regime classification of the labile and the stable regime and a figure each representing a moment of the temperature distribution [22].

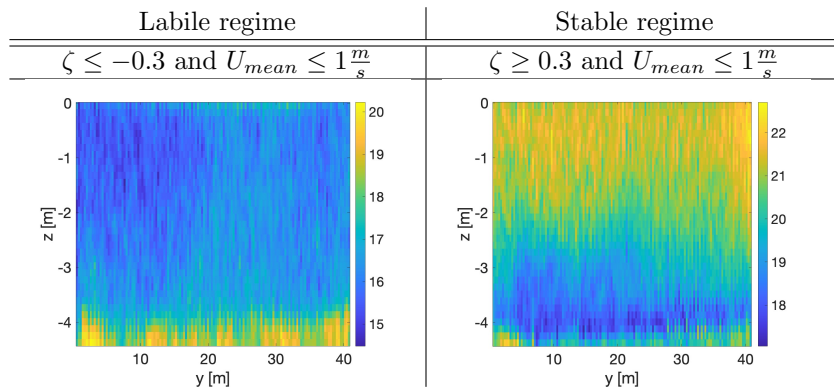


Table 1: Regime classification for the labile and the stable regime. The figures of the temperature distribution are plotted along the height and the y-axis of the measurement structure. The chosen moment of time for each figure is representative for each regime. The figure (a) displays the data for the labile regime of the No.19, 09:03h and the data for figure (b) was measured in the stable regime of the data set No.23, 20:03h

In the following tables the starting points of time of the 60-minute data sets fulfilling the above described restrictions are listed for each the labile (in table 2) and the stable regime (in table ??) including the values of zeta, the offset angle between the measurement fibre, the measured mean velocity U_{meas} and the standard derivation of the measured crosswind velocity V_{meas} , representing the sweeping velocity.

No.	Date	Angle [°]	Zeta	U_{meas} [m/s]	V_{meas} [m/s]
1	28.08. 07	11	-0.38	0.3	0.37
2	28.08. 10	357	-0.35	0.64	0.85
3	04.09. 09	185	-1.7	0.86	0.54
4	07.09. 08	198	-0.39	0.59	0.44
5	07.09. 11	199	-1.29	0.5	0.71
6	08.09. 09	188	-1.28	0.54	0.56
7	12.09. 14	194	-0.96	0.95	0.77
8	13.09. 09	190	-0.96	0.52	0.49
9	15.09. 09	190	-0.9	0.4	0.67
10	16.09. 09	19	-0.53	0.44	0.52
11	16.09. 12	10	-0.31	0.58	0.88
12	16.09. 13	20	-0.3	0.86	0.84
13	20.09. 09	15	-0.47	0.77	0.65
14	20.09. 12	4	-1.79	0.21	0.81
15	22.09. 12	188	-1.54	0.64	0.59
16	22.09. 13	199	-0.46	0.8	0.5
17	23.09. 07	199	-0.36	0.85	0.5
18	23.09. 09	175	-0.87	0.57	0.58
19	24.09. 09	175	-0.63	0.95	0.61
20	29.09. 12	18	-0.78	0.89	0.73
21	30.09. 09	175	-1.27	0.68	0.55
22	01.10. 08	193	-0.4	0.76	0.29
23	02.10. 08	186	-0.36	0.9	0.47
24	06.10. 12	195	-0.45	0.74	0.62

Table 2: Table of data sets fulfilling the restrictions for the labile regime. The date represents the day and the starting point of time of the one hour data set, the angle representing the offset angle between the measurement fibre and the wind direction, the measured mean velocity U_{meas} represents the average velocity over one hour each. V_{meas} is the standard derivation of the crosswind velocity.

No.	Date	Angle [°]	Zeta	U_{meas} [m/s]	V_{meas} [m/s]
25	04.09. 22	355	0.63	0.22	0.23
26	09.09. 20	199	0.38	0.31	0.25
27	09.09. 23	181	0.72	0.4	0.18
28	10.09. 18	1	0.51	0.67	0.29
29	10.09. 22	176	0.49	0.63	0.23
30	15.09. 21	13	0.44	0.05	0.43
31	15.09. 22	13	0.36	0.2	0.22
32	19.09. 19	10	0.43	0.41	0.3
33	23.09. 00	175	0.66	0.84	0.28
34	23.09. 01	191	0.35	0.29	0.46
35	23.09. 20	198	0.41	0.85	0.25
36	24.09. 02	182	0.73	0.15	0.16
37	28.09. 20	185	0.4	0.12	0.18

Table 3: Table of data sets fulfilling the restrictions for the stable regime. The date represents the day and the starting point of time of the one hour data package, the angle representing the offset angle between the measurement fibre and the wind direction, the measured mean velocity U_{meas} represents the average velocity over one hour each. V_{meas} is the standard derivation of the crosswind velocity.

5.2 Wavelet high-pass filtering applied prior to analysis

The motivation for applying a preliminary filtering function to the data is the importance of selecting the scales of turbulence only.

The surface heating as a result of the incoming solar radiation during the day produces motions

larger than those typically found in atmospheric turbulence, which creates lower frequency contributions in empirical power spectra of air temperature and wind velocity components.

To limit the significant temperature changes at the turbulence time scales, a wavelet high-pass filter is applied to the FODS temperature data [21] prior to further analysis. The wavelet function is “a bandpass filter of uniform shape and varying location and width” [23] and enables one to “unfold a signal into both space and scale” [24]. This is done “by decomposing a time series into time–frequency space to determine both the dominant modes of variability and how those modes vary in time” [23].

The wavelet filter applied for this analysis is based on the biorthogonal set of wavelets BIOR5.5, which is used for “separating the low frequencies of coherent motion from high frequent turbulence” [25]. By comparing the unfiltered and filtered generated signal with steadily increasing parameter a , one can evidently notice that the wavelet filter divides the oscillations to the lower frequencies and higher frequencies depending on the wavelet scale a .

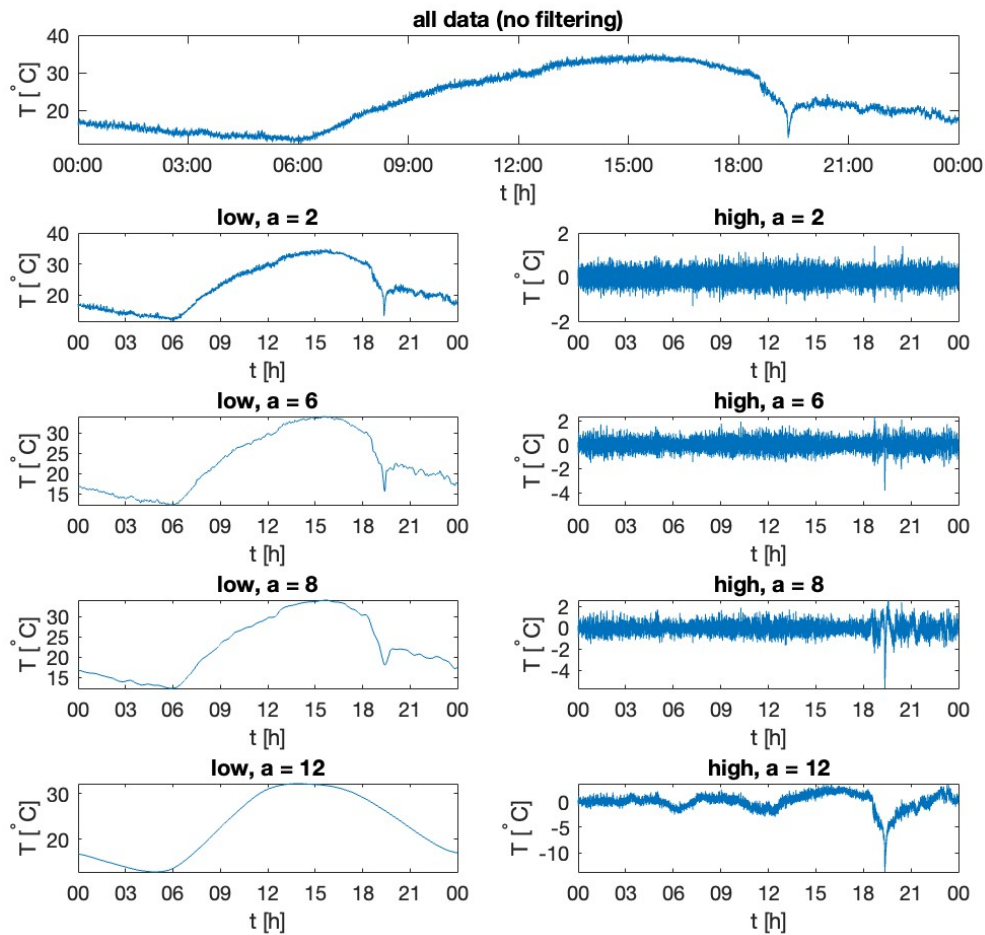


Figure 3: Temperature course after high and low pass filtering for different parameter a of the day 10.09.2011 which is a representative daily course for the display of this application)

In this figure 3 of the temperature course one can conclude that the main warming signal is directly related to the daily course of the sun. Due to the indirect proportionality of time range length and frequencies, the lower frequencies represent the daily course and therefore include the incoming solar forcing. Separating the high frequencies from the low frequencies by applying the wavelet function, is therefore leading to a separation of the incoming energy and the high frequency turbulent range.

For the justification of the choice of the value of the wavelet parameter a , the power spectrum of

the data is shown. As discussed in the section before, the dissipation range equals a decay of the power spectrum of the value $-5/3$, which also should be seen in the power spectrum of the data. The following figure show the power spectrum of temporal fluctuating temperature calculated from the measured data before and after the usage of the wavelet bandpass filter with the parameter a .

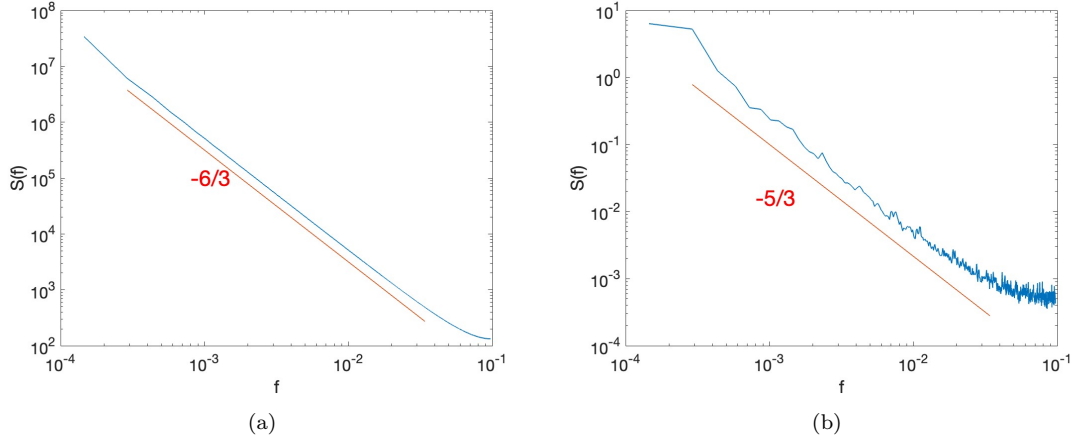


Figure 4: Averaged power spectrum of temporal fluctuating temperature calculated from the measured data sets in the labile regime. The average was calculated over all data sets in the labile regime. The figures show the averaged power spectrum a) before and b) after the wavelet application with the wavelet parameter $a = 12$.

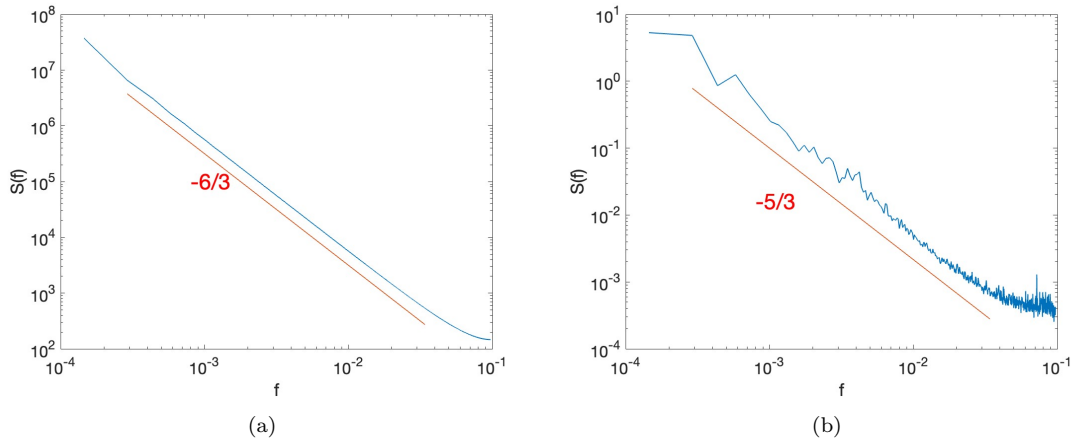


Figure 5: Averaged power spectrum of temporal fluctuating temperature calculated from the measured data sets in the stable regime. The average was calculated over all data sets in the stable regime. The figures show the averaged power spectrum a) before and b) after the wavelet application with the wavelet parameter $a = 12$.

As we now have evidence that the separated high-pass filtered air temperature observations represent atmospheric turbulence, we can now start the analysis of the spatio-temporal correlation of the multi-point temperature data measured by FODS [20].

6 Methods

In this section, the methods of deriving the characteristic parameters of the elliptic model, the convection velocity U and the sweeping velocity V , are explained in detail. In this paper we follow two different methods to derive these parameters. For traceability the parameters will have indices that clarifies the origin of its derivation method. First we will obtain the parameters U_m and V_m with the maxima fit method, by using a maxima determination, for which the paper [6] by Han and Zhang is being followed. Secondly, the parameters U_e and V_e are determined by fitting an ellipse to the iso-correlation contour lines and extracting the parameters by calculation from the characteristic elliptic values. I will name this method elliptic fit method from now on. The motivation behind this method is, that the elliptic model states that the iso-contour lines equal oblique ellipses. Therefore we can describe the contour lines with the equation $r_c^2 = (r - U \cdot \tau)^2 + (V \cdot \tau)^2$, where r_c is the point on the r -axis, where the ellipse cuts the axis. This relation has been described and discussed in the section Theoretical Part before, where you can find further information in more detail.

As both methods are based on the correlation function, the spatio-temporal correlation $C(x, \tau)$ is described upfront. In the section experimental set up, I explained that the data we use is temporal fluctuating data. Therefore the spatio-temporal correlation represents the autocorrelation of the temporal fluctuating data the correlation function. To clarify this connection, I will use the label 'TT' along the correlation function. Therefore $C(r, \tau) = C_{TT}(r, \tau)$. The expression for $C_{TT}(r, \tau)$ is given by

$$C_{TT}(r, \tau) = \left\langle \frac{\langle T(x, t)T(x+r, t+\tau) \rangle_t}{\sqrt{\text{Var}(T(x))}\sqrt{\text{Var}(T(x+r))}} \right\rangle_x \quad (18)$$

Based on the assumption of statistically steady and homogeneous fluctuations, temporal and spatial averaging is applied to the correlation function, which is indicated with $\langle \rangle_t$ and $\langle \rangle_x$. Important here is to state, that the correlation function is taken at every single measurement point in both directions along the measurement cable. This leads to different numbers of correlation samples for different spatial spacing. For example we have 138 correlation samples for the spatial spacing $r = 0\text{m}$ and only one for each $r = \pm 40\text{m}$. So the averaging was done by dividing each summed value for the specific r with the numbers of resulted correlation functions.

The correlation function is also standardised, which leads to the advantage of better comparison between the correlation results of the data sets.

Due to its dependence on r and τ , the correlation function $C_{TT}(r, \tau)$ can be plotted in a 3-dimensional plot or can be visualised in its contour plot. The contour plot is used as the basis for the further analysis.

The figures in this section are chosen for their visualisation of the explanations of the models.

6.1 Extraction of parameters U_m and V_m using a maxima determination

For the velocity calculation based on the extraction of the parameters U_m and V_m by using a maxima determination we follow the steps in the paper [6] by Han and Zhang. It is important to be aware of the renaming that was made in comparison to the paper.

The parameters U_m and V_m can be derived from the relation of the elliptic model $r_c^2 = (r - U_m\tau)^2 + (V_m\tau)^2$. We can get the velocity U_m via

$$\left. \frac{\delta r_c}{\delta r} \right|_{\tau} = 0 \quad \rightarrow \quad \tau = C_U r_p = \frac{1}{U_m} r_p \quad (19)$$

The variable r_p represents the spatial shift r that maximizes $C_{TT}(r, \tau)$ for a constant τ . The requirement of τ being constant is defined by the mathematical spelling $|_{\tau}$. We will see later on, that U_m can be obtained from the gradient C_U with the relation $U_m = 1/C_U$ when we plot r_p against τ . We follow a similar path for the derivation of the sweeping velocity V_e , thus

$$\left. \frac{\delta r_c}{\delta \tau} \right|_r = 0 \quad \rightarrow \quad \tau_p = C_V r = \left[\frac{U_m}{(U_m^2 + V_m^2)} \right] r \quad (20)$$

where τ_p maximizes $C_{TT}(r, \tau)$ for a given r . Similar to above, the spelling $|_r$ states that r is required to be constant and we can obtain V from the gradient $C_V = \frac{U_m}{(U_m^2 + V_m^2)}$, by plotting r against τ_p .

The actual implementation is as follows: To obtain the gradient C_V in equ. (20), we plot the correlation function $C_{TT}(r, \tau)$ of various specific r against the time shift τ . Analog we plot $C_{TT}(r, \tau)$ of various specific τ against the spatial shift r to receive the gradient C_U in equ. (19). Therefore both equations imply keeping one variable (r , respectively τ) fixed while plotting the correlation function against the other variable (τ , respectively r).

Conceptually we can break down this approach to the illustration of a grid overlay to the iso-correlation contour lines, which you can see in the following figure, where the red lines represent the fixed values of r in fig. 6a, respectively τ in fig. 6b.

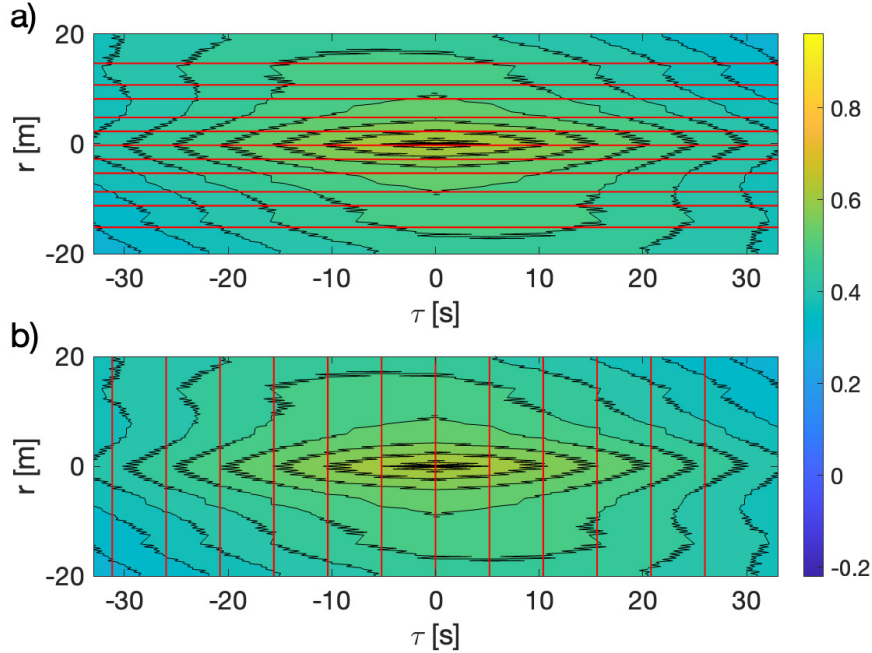


Figure 6: Illustration of the concept behind the approach of plotting the Correlation function $C_{TT}(r, \tau)$ versus r respectively τ to obtain the velocity parameters U_m and V_m . The black lines represent the iso-correlation contour lines that enclose areas of the same correlation value. The correlation values of the colors of the areas are displayed in the color bar on the right. In a) the red lines represent the correlation function $C_{TT}(r, \tau)$ with a fixed spatial shift value r , plotted against τ . Displayed are the values $r = [0m, \pm 5.1m, \pm 8.5m, \pm 11m, \pm 15m, \pm 17.5m]$ In b) the red lines represent the correlation function $C_{TT}(r, \tau)$ with a fixed value of τ plotted against the spatial shift r . Displayed are the temporal shift values $\tau = [0s, \pm 5.2s, \pm 10.3s, \pm 15.5s, \pm 20.7s, \pm 25.9s]$

The conceptual approaches of obtaining the coefficients C_V and C_U are done analogously. Therefore we will only focus on the approach of receiving the coefficient C_V in this methodical description. In a first step, the correlation function $C_{TT}(r, \tau)$ is plotted against the temporal spacing τ for different constant values of r , which can be seen in figure 7. In a second step, we apply a parabola fit function to the correlation function of each values of r to obtain its maximum. The τ -position of the correlation maximum represents the wanted value of τ_p . I visualised this approach in the figure 8. In this figure we can also see that the correlation functions drop to different degrees and therefore are partly very pointed. For these cases the fitted parabola does not represent the correlation value perfectly. But as we only need the value of τ for the different correlation functions $C_{TT}(r, \tau)$, this approach leads to the valid parameters τ_p . In the last step of the maxima fit method we plot the measured peak position τ_p as a function of r and apply a linear fit to the scatter plot to obtain the gradient C_V . The choice of the linear regression fit is based on the expectation that the relation of r and τ_p is linear increasing for increasing values of r . I use the implemented MatLab function `fitlm` as the linear regression fit. This whole procedure was repeated for obtaining the value of the gradient C_U . We can now calculate U_m and V_m by using the equations (19) and (20) and the obtained values of C_U and C_V . The r - τ_p plot and the linear

regression fit as well as the calculated values of U_m and V_m can be found in the result section. To improve the results of the to parameters, I applied the limitation to the maximum value of $C_{TT}(r, \tau) > 0.2$. This leads to a limitation to the used range of the spatial and temporal shift values for the data sets.

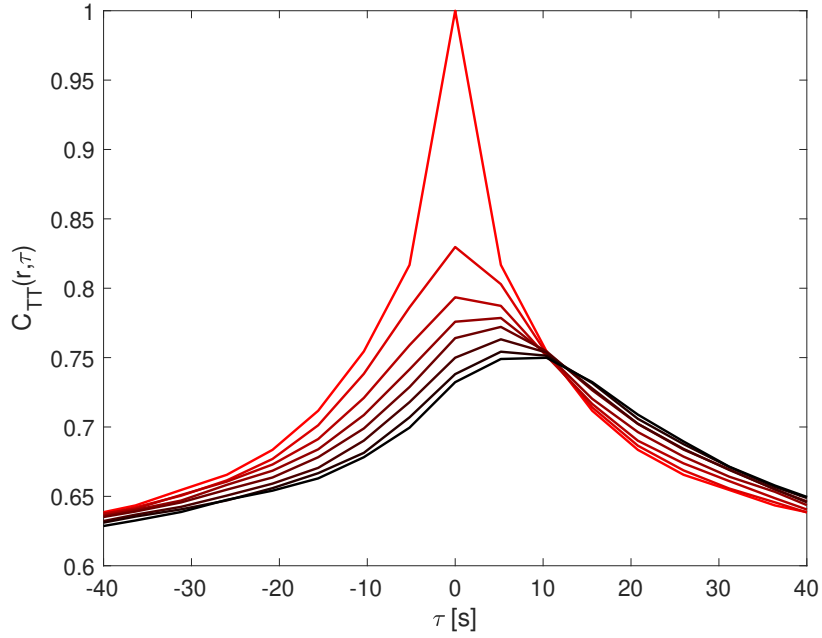


Figure 7: Space-time correlation $C_{TT}(r, \tau)$ of the data No.19 for different values of r plotted against τ . The higher the value of r the darker its correlation function line. The values of r are: $r = [0\text{m}, 1.27\text{m}, 2.54\text{m}, 3.81\text{m}, 5.08\text{m}, 6.35\text{m}, 7.26\text{m}, 8.25\text{m}]$. For clarity this figure only shows the positive r values.

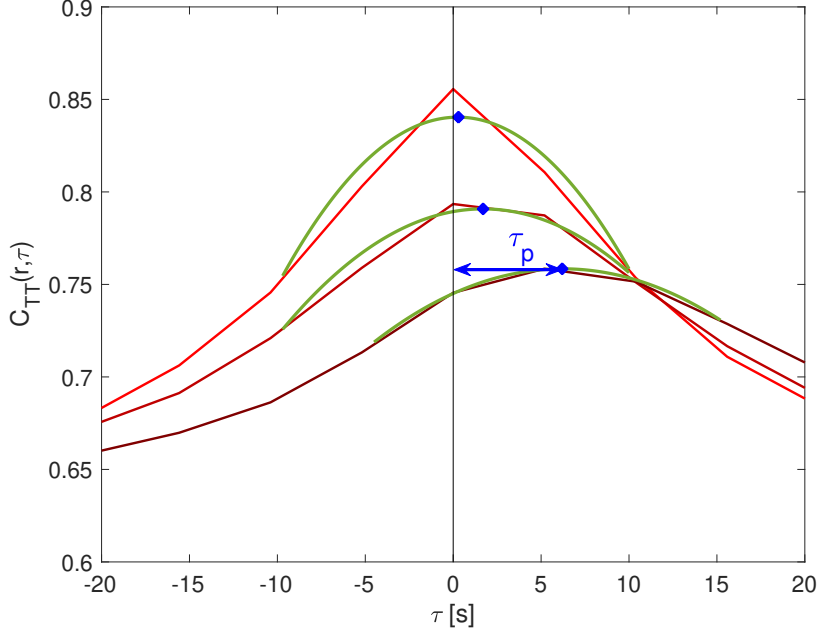


Figure 8: Parabola fit to $C_{TT}(r, \tau)$ of data set No.19 for different values of r to obtain the maximum. The red graphs represent the correlation function $C_{TT}(r, \tau)$ for different values of r plotted against τ . The higher the value of r the darker its correlation function line. The values of r displayed are: $r = [0.95\text{m}, 2.54\text{m}, 7.26\text{m}]$. The green lines are the parabola fit with their marked maximum as a blue star. The horizontal distance of the maximum to the value $\tau = 0$ represents the value of τ_p

6.2 Extraction of parameter U_e and V_e by fitting an ellipse to the iso-contour lines of the correlation function

The second method of deriving the values of U_e and V_e is the elliptic fit method. The motivation of the method is based on the assumption of the elliptic model, that the iso-contour lines of the spatio-temporal correlation are elliptic shaped with an expansion and orientation connected to the parameters U_e and V_e . To extract the ellipse parameters, an ellipse is fitted to an iso-correlation contour line. The approach can be seen in the figure 9.

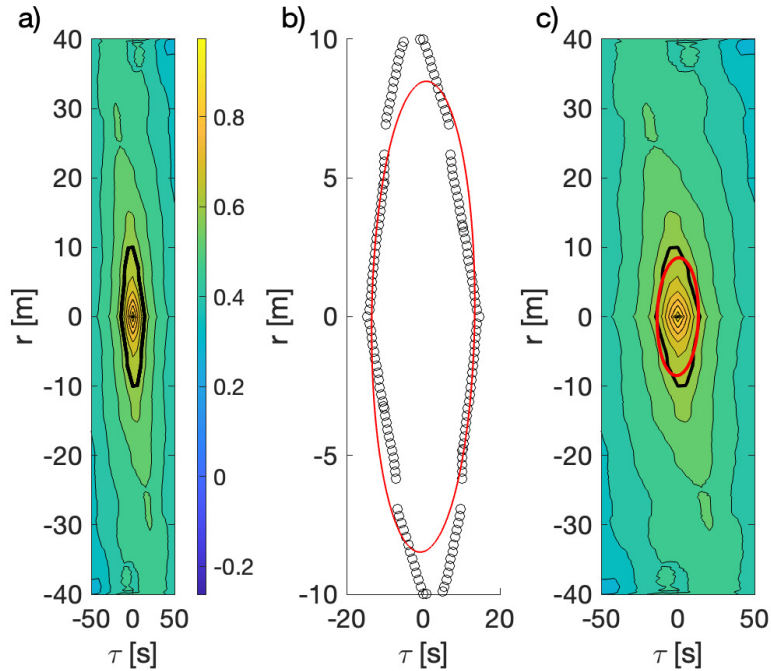


Figure 9: Conceptual description of the elliptic fit method. The exemplary correlation function used in this figure is the data set No. 16. In the subfigure a) we can see the iso-contour plot of the correlation function with a highlighted contour line of the value $C_{TT}(r, \tau)=0.62$ marked as a thick black line. In b) the iso-contour points representing the line are plotted as black circled dot. The red ellipse is the elliptic fit. In c) we can see the same iso-correlation contour plot as in a) with the elliptic fit in red.

The operating principles of the elliptic fit is based on a minimization concept. The sum of the quadratic distance between the points on the iso-contour and the values of the elliptic fit is minimised in both the horizontal and vertical direction. The fit goes through several iterations. The elliptic fit then outputs the parameters a and b of the two semi-axes and the value of the angle α by which the fitted ellipse is rotated against the horizontal axis.

We apply the elliptic fit to several iso-correlation contour lines. The correlation value range for the application is determined as follows: The minimum value was elected by the biggest enclosed iso-contour line of the iso-correlation contour plot. I chose the maximum of the correlation contour value by containing a minimum of 10 points. I divided the range into 40 equally spaced iso-contour values and applied the elliptic fit to each value. We can see the application of the elliptic fit method with all 40 fitted ellipses in figure 10. We calculate the value of U_e^* and V_e^* for each fitted ellipse and average it for each data set. The designation * marks that the parameters of U_e^* and V_e^* are the result of a single fitted ellipse. After calculating all values, we take the mean of U_e^* and V_e^* , which leads to the representative value $\bar{V}_e = V_e$ and $\bar{U}_e = U_e$ for each data set. I did the renaming for better clarification in the discussion section.

For the calculation of U_e^* and V_e^* we start with the conversion of the elliptic parametric form into the normal form. We can describe an oblique ellipse as an ellipse with its semi axes a and b which is transformed by a rotation matrix Z by the angle α . We can write the relation in the parametric form as

$$\begin{pmatrix} \tau \\ r \end{pmatrix} = \begin{pmatrix} \cos \alpha & -\sin \alpha \\ \sin \alpha & \cos \alpha \end{pmatrix} \cdot \begin{pmatrix} a \cos t \\ b \sin t \end{pmatrix} = Z \cdot \begin{pmatrix} x \\ y \end{pmatrix}, \quad (21)$$

where the vector $(x \ y)^T$ describes the unrotated ellipse with the same semi-axes a and b . We can now rewrite the equation to receive the normal form of the oblique ellipse. To do so, the Matrix Z is inverted leading to the relation:

$$\begin{pmatrix} a \cos t \\ b \sin t \end{pmatrix} = \begin{pmatrix} \cos \alpha & \sin \alpha \\ -\sin \alpha & \cos \alpha \end{pmatrix} \cdot \begin{pmatrix} \tau \\ r \end{pmatrix} \quad (22)$$

We divide by the values of the semi axes a as well as b and take its absolute value, which leads us

to the relation

$$1 = \left(\frac{\sin^2 \alpha}{a^2} + \frac{\cos^2 \alpha}{b^2}\right)r^2 + \left(\frac{2 \cos \alpha \sin \alpha}{a^2} - \frac{2 \sin \alpha \cos \alpha}{b^2}\right)\tau r + \left(\frac{\cos^2 \alpha}{a^2} + \frac{\sin^2 \alpha}{b^2}\right)\tau^2. \quad (23)$$

We now rewrite the equation (12) stated by the elliptic model to

$$r_c^2 = r^2 - 2U_e^* r \tau + (U_e^{*2} + V_e^{*2})\tau \quad (24)$$

which is rewritten to:

$$1 = \frac{1}{r_c^2}r^2 - \frac{2U_e^* r \tau}{r_c^2} + \frac{(U_e^{*2} + V_e^{*2})}{r_c^2}\tau \quad (25)$$

The comparison leads us now to the following relations:

$$\frac{1}{r_c^2} = \left(\frac{\sin^2 \alpha}{a^2} + \frac{\cos^2 \alpha}{b^2}\right) \quad (26)$$

$$U_e^* = r_c^2 \cos \alpha \sin \alpha \left(\frac{1}{a^2} - \frac{1}{b^2}\right) \quad (27)$$

$$V_e^* = \sqrt{\left(\frac{\cos^2 \alpha}{a^2} + \frac{\sin^2 \alpha}{b^2}\right) \cdot r_c^2 - U_e^{*2}} \quad (28)$$

The averaging of all calculated parameters V_e^* and U_e^* leads us to the following equations:

$$V_e = \frac{1}{40} \sum_{i=1}^{40} V_{ei}^* \quad (29)$$

$$U_e = \frac{1}{40} \sum_{i=1}^{40} U_{ei}^* \quad (30)$$

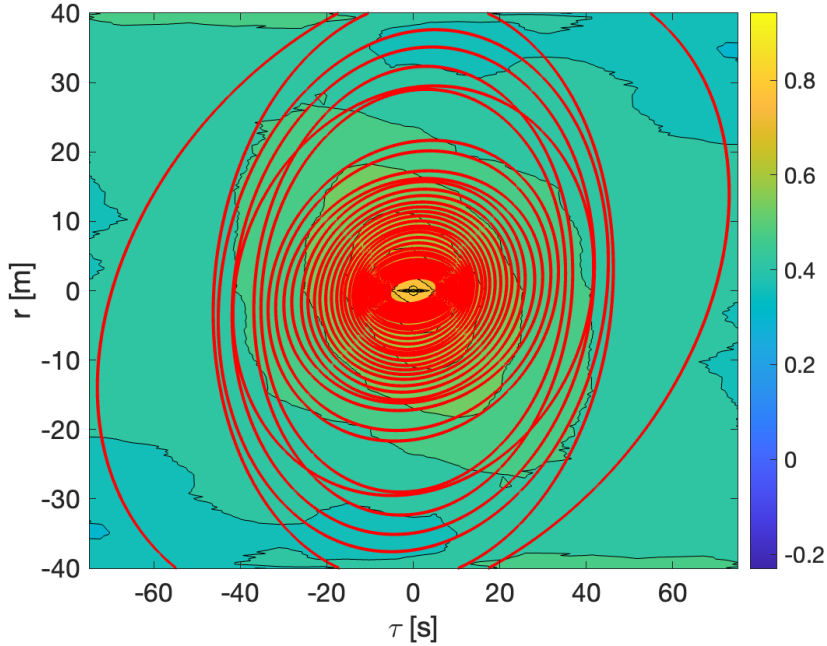


Figure 10: Application of the elliptic fit method to the iso-correlation contour plot of the data No.2. The red ellipses represent the elliptic fits fitted to equally spaced iso-contour values. The determined correlation-value-range is $C_{TT}(r, \tau) = [0.43 : 0.85]$.

7 Results

I will first display the different types of the correlation patterns seen in the data. Then I will present the calculated velocities U_m and V_m of the maxima fit method and the calculated velocities U_e and V_e of the elliptic fit method.

7.1 Characteristic types of iso-contour plots

In figure 11 an iso-correlation contour plot with elliptic shaped iso-contour lines is displayed. The correlation value ranges from 0.1 to 1. The iso-correlation contour lines represent elliptic shaped lines. In figure 12(a) we can see a sharp correlation value, from $C_{TT}(r, \tau) = 1$ to $C_{TT}(r, \tau) = 0.3$ in less than $r = 0.25\text{m}$ and less than $\tau = 5\text{s}$. A very slow drop of the correlation value can be seen in figure 12(a). For some correlation functions the iso-contour lines differ from elliptic shaped lines. In the figure 13(a) we can see an iso-correlation contour plot that shows almost no spatio correlation, leading to straight contour lines parallel to the spatio axis. This iso-correlation contour pattern applies to the data of No.1, No.3 and No.28. A correlation function that shows no visible correlation can be seen in the figure 13(b). This iso-correlation contour pattern can be found in the data set No.4, No.5, No.6.

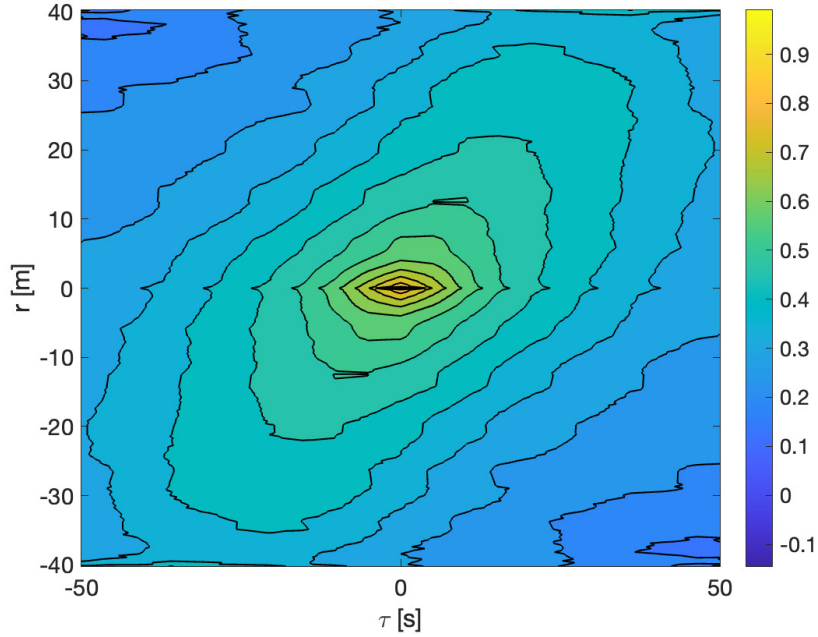


Figure 11: Iso-correlation contour pattern of the correlation $C_{TT}(r, \tau)$ of the data No. 15. The maximum value of the $C_{TT}(r, \tau)$ occurs at the origin with $C_{TT}(0, 0) = 1$. The two-dimensional iso-contour lines of the measured correlation function form elliptic shaped enclosed lines. The value of the $C_{TT}(r, \tau)$ declines with increasing separation of r respectively τ .

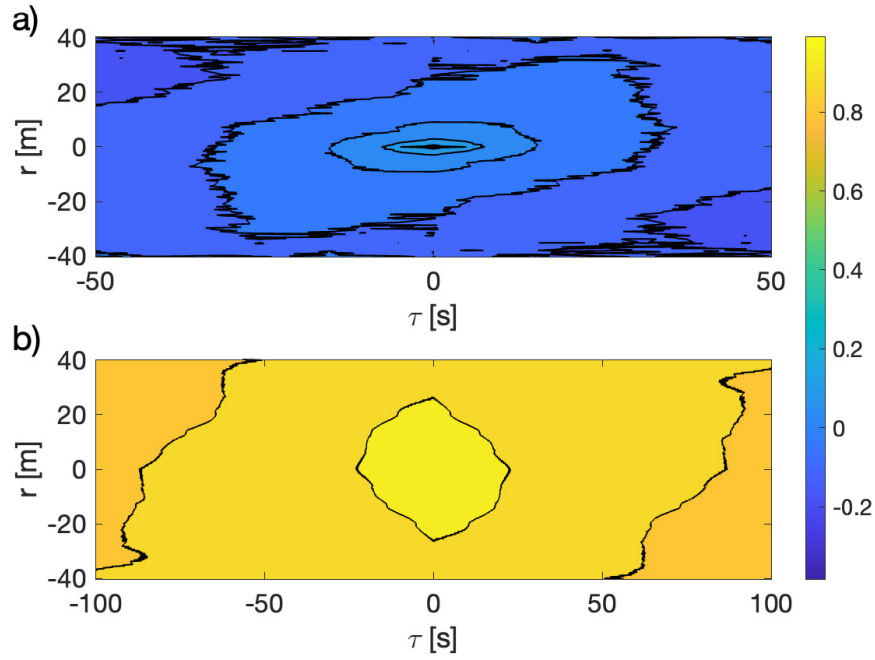


Figure 12: Iso-correlation contour pattern. The black lines are the iso-contour lines separating the areas of the same correlation value. The color bar represents the values of the correlation function ranging from -0.4 to 1.

- a) Iso-contour pattern of the correlation function $C_{TT}(r, \tau)$ data of No 8.
 b) Iso-contour pattern of the correlation function $C_{TT}(r, \tau)$ of No 24.

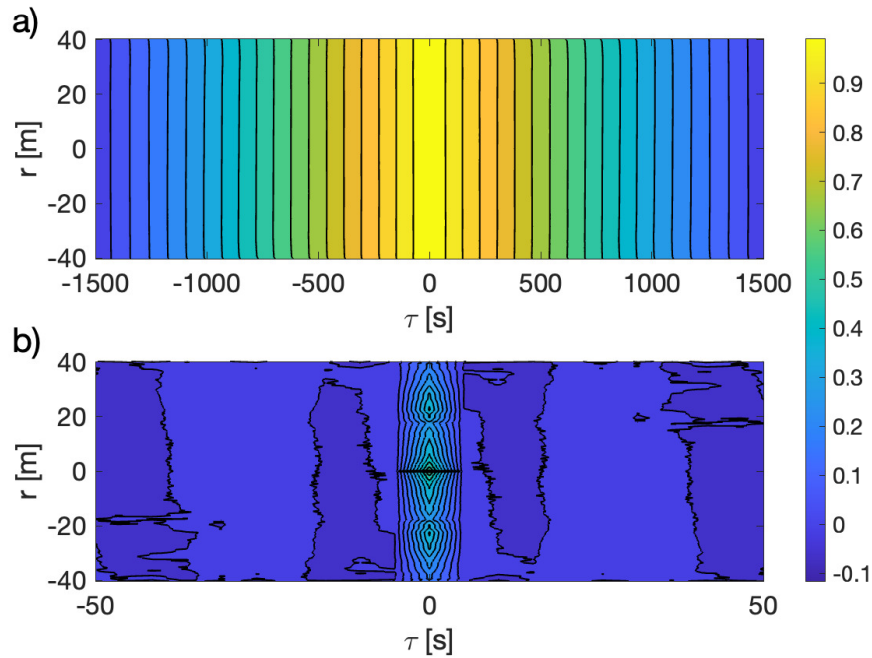


Figure 13: Iso-contour plot of the correlation function $C_{TT}(r, \tau)$. The black lines are the iso-contour lines separating the areas of the same correlation value. The color bar represents the values of the correlation function ranging from -0.1 to 1.

- a) Iso-contour plot of the correlation function $C_{TT}(r, \tau)$ of the data No.3 in the labile regime.
 b) Iso-contour plot of the correlation function $C_{TT}(r, \tau)$ of data No. 5 in the labile regime.

7.2 Results of parameters U_m and V_m using the maxima determination method

The results for the specific streamwise spacing r plotted versus its corresponding value of τ_p is illustrated in the figure 14(a) for the labile regime and in figure 15(a) for the stable regime. It shows a linear increase of r with increasing τ_p . A linear regression fit of MatLab called fitlm was used to determine the gradient coefficient $C_V = r/\tau_p$. This procedure was also done for the maximum value of $C_{TT}(r, \tau)$ for various temporal spacings τ resulting in the gradient coefficient $C_U = \tau/r_p$ and can be seen in the figures 14(b) and figure 15(b) These values of the gradient coefficients can be calculated into the values of U_m and V_m with the equations (19) respectively (20). The errors for the values U_m and V_m were calculated by the fit function. We can find the values of the data sets representing the labile regime in table 4 and the stable regime in table 5.

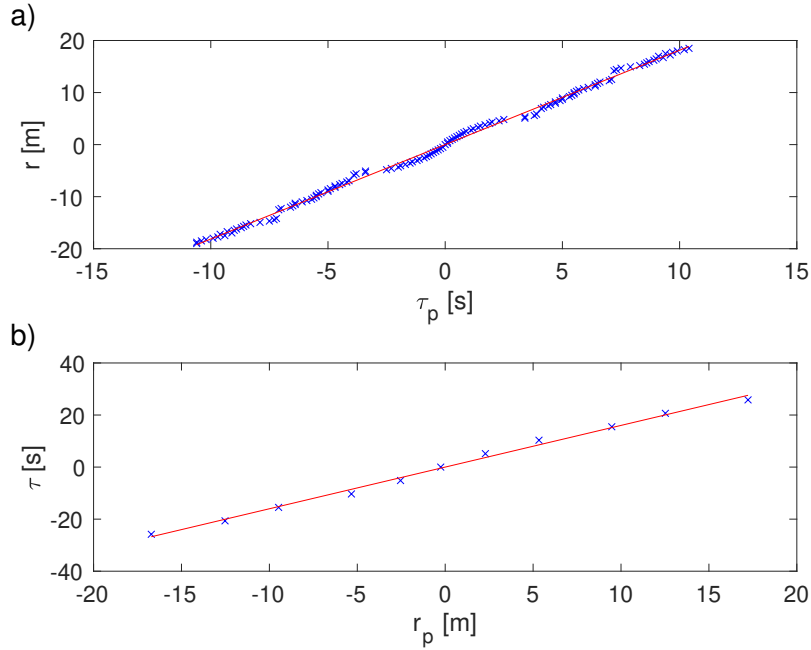


Figure 14: Result of the application of the maxima fit method to the data set No.16 in the labile regime. a) Spatial shift r versus τ_p . The blue crosses represent each the temporal spacing τ_p which maximises the correlation function $C_{TT}(r, \tau)$ for specific values of streamwise spacing r . The red line is a linear fit to these data points. The fit is done with the prefabricated fit function fitlm in MatLab. The fit returns the value of the gradient coefficient $C_V = r/\tau_p$ and its error. b) Temporal shift τ versus r_p . The blue crosses represent each the spatial spacing r_p that maximises the correlation function $C_{TT}(r, \tau)$ for the values of specific temporal shifts τ . The red line is a linear fit to these data points. The fit is done with the prefabricated fit function fitlm in MatLab. The fit returns the value of the gradient coefficient $C_U = \tau/r_p$ and its error.

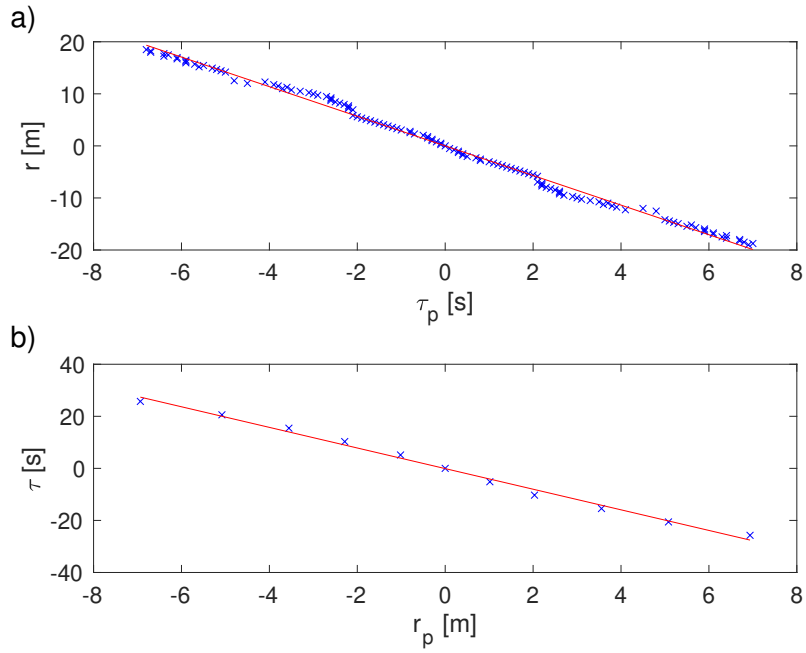


Figure 15: Result of the application of the maxima fit method to the data set No.26 in the stable regime. a) Spatial shift r versus τ_p . The blue crosses represent each the temporal spacing τ_p which maximises the correlation function $C_{TT}(r, \tau)$ for specific values of streamwise spacing r . The red line is a linear fit to these data points. The fit is done with the prefabricated fit function `fitlm` in MatLab. The fit returns the value of the gradient coefficient $C_V = r/\tau_p$ and its error. b) Temporal shift τ versus r_p . The blue crosses represent each the spatial spacing r_p that maximises the correlation function $C_{TT}(r, \tau)$ for a values of specific temporal shifts τ . The red line is a linear fit to these data points. The fit is done with the prefabricated fit function `fitlm` in MatLab. The fit returns the value of the gradient coefficient $C_V = r/\tau_p$ and its error.

No	U_m	$Error_U$	V_m	$Error_V$
1	-0.09	1.88	1.03	0.70
2	-0.16	0.25	0.56	0.02
3	-1.40	0.56	13.28	9.10
4	121.02	0.37	138.06	24.88
5	-19.49	0.31	31.05	0.96
6	-5.52	0.33	24.04	6.46
7	0.30	0.47	1.11	0.17
8	0.24	0.14	0.68	0.08
9	0.30	0.19	0.83	0.10
10	-0.26	0.24	0.75	0.04
11	-0.16	0.36	0.67	0.07
12	-0.66	0.09	1.00	0.02
13	-0.52	0.12	0.96	0.21
14	-0.24	0.61	0.67	0.09
15	0.54	0.06	0.74	0.02
16	0.63	0.04	0.86	0.01
17	0.16	1.26	0.63	0.08
18	0.20	0.73	0.85	0.04
19	0.89	0.10	1.16	0.01
20	-0.17	1.47	0.57	0.02
21	0.54	0.04	1.06	0.21
22	0.26	0.22	0.82	0.21
23	0.41	0.09	1.29	0.18
24	0.20	0.40	0.96	0.05

Table 4: Values of the calculated velocities U_m , V_m and their errors E_U and E_V calculated using the maxima fit method for the data sets conducted in the labile regime

No	U_m	$Error_U$	V_m	$Error_V$
25	0.06	1.18	0.56	0.64
26	-0.25	0.11	0.81	0.02
27	-0.18	0.30	1.15	0.08
28	-0.12	0.67	0.95	0.07
29	-0.36	0.20	0.70	0.05
30	-0.08	1.20	0.57	0.57
31	0.04	1.89	0.51	0.39
32	-0.04	5.52	0.53	0.45
33	0.29	0.18	0.87	0.05
34	0.06	0.78	0.65	0.42
35	0.05	6.65	0.61	0.27
36	-0.15	0.44	1.27	0.28
37	-0.20	0.18	0.79	0.09

Table 5: Values of the calculated velocities U_m , V_m and their errors E_U and E_V calculated using the maxima fit method for the data sets conducted in the stable regime

7.3 Results of the values U_e and V_e extracted by the ellipse fit method

Before displaying the results for U_e and V_e conducted with the elliptic method, I would like to point out this method is not applicable to the correlation function of some data sets. The requirement of the elliptic fit method are elliptic shaped iso-contour lines to which the elliptic fit can be applied. We can find the iso-correlation contour patterns that are unfitting for this method in figure 13(a) and 13(b) as the iso-contour lines of these patterns don't fulfil the requirement. Due to the impossibility of applying this method to these iso-correlation contour plots, the data of No.1, No.3, No.4, No.5 and No.6 are left for the analysis using the elliptic fit method.

As explained in detail in the Method section, I determined a range of $C_{TT}(r, \tau)$ for every data

set suitable for applying the elliptic fit method. In this range I applied the elliptic fit to 40 equally spaced iso-correlation contours, resulting in values for U_e and V_e for specific correlation values, which are calculated with the equations (27) and (28) and displayed in the figure 16. The red dots describe the values of $U_e(C_{TT})$ and $V_e(C_{TT})$ and the blue horizontal line represents the mean value of V_e or U_e . For every data set, the calculated values U_e and V_e were averaged resulting in the mean velocity $\overline{U_e}$ and sweeping velocity $\overline{V_e}$. We can find these averaged velocities $\overline{U_e}$ and $\overline{V_e}$ in the table 6 for the labile regime and in the table 7.

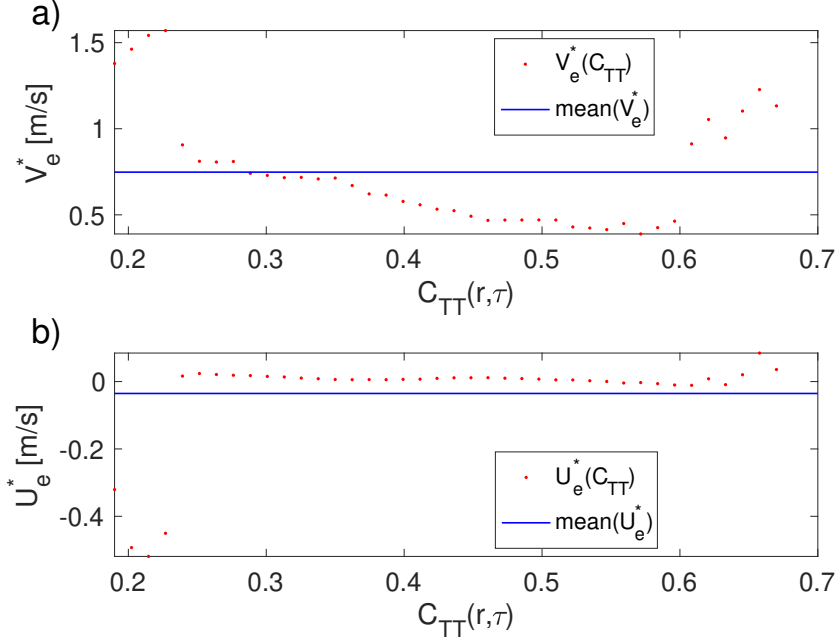


Figure 16: Calculated values of $U_e(C_{TT})$ and $V_e(C_{TT})$ of the data No.2 in the labile regime. The minimum of the range of $C_{TT}(r, \tau)$ was determined by the lowest value that provides an enclosed line, the maximum was determined by the maximum value of the contour line that consists of a minimum of 10 data points.

a) The red dots are the value of $V_e(C_{TT})$ calculated with the equation (28). The blue line is the $\overline{V_e}$, the average of V_e .

a) The red dots are the value of $U_e(C_{TT})$ calculated with the equation 27. The blue line represents $\overline{U_e}$, the average of U_e .

No.	\overline{U}_e	\overline{U}_{std}	\overline{V}_e	\overline{V}_{std}
2	-0.06	0.03	0.6	0.2
7	-0.04	0.14	0.7	0.3
8	-0.02	0.10	0.6	0.3
9	0.03	0.03	0.6	0.2
10	-0.01	0.04	0.5	0.2
11	-0.02	0.04	0.6	0.3
12	0.05	0.16	0.9	0.4
13	-0.05	0.05	0.7	0.3
14	0.00	0.13	0.5	0.3
15	-0.01	0.08	0.7	0.3
16	-0.1	0.23	0.8	0.4
17	-0.03	0.07	0.7	0.4
18	-0.01	0.06	0.8	0.4
19	-0.28	0.41	1.2	0.4
20	-0.04	0.05	0.7	0.2
21	-0.04	0.12	0.9	0.4
22	0.02	0.14	0.7	0.7
23	-0.02	0.05	0.9	0.3
24	0.00	0.09	0.8	0.4

Table 6: Results of the averaged \overline{V}_e and \overline{U}_e calculated by using the elliptic fit model of the data sets in the labile regime.

No.1, No.3, No.4, No.5 and No.6 are not listed here, as their resulting iso-correlation contour plot doesn't fulfill the requirement of elliptic shaped iso-contour lines for the elliptic fit method, which leads to the impossibility of applying this method to their iso-correlation contour plots.

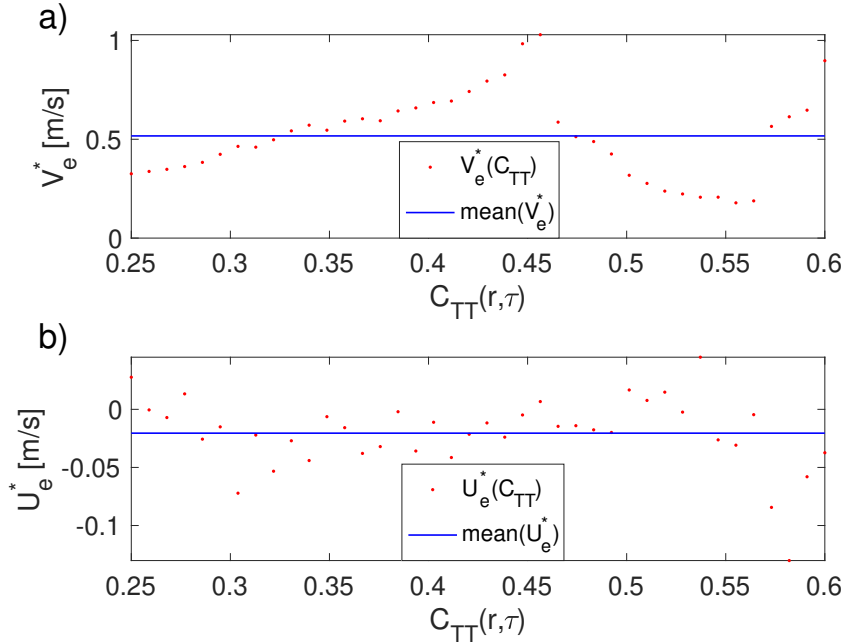


Figure 17: Calculated values of $U_e(C_{TT})$ and $V_e(C_{TT})$ of the data No. 26 in the labile regime. The minimum of the range of $C_{TT}(r, \tau)$ was determined by the lowest value that provides an enclosed line, the maximum was determined by the maximum value of the contour line that consists of a minimum of 10 data points.

a) The red dots are the value of $V_e(C_{TT})$ calculated with the equation (28). The blue line is \overline{V}_e , the average of V_e .

a) The red dots are the value of $U_e(C_{TT})$ calculated with the equation (27). The blue line represents \overline{U}_e , the average of U_e .

No.	\overline{U}_e	\overline{U}_{std}	\overline{V}_e	\overline{V}_{std}
25	0.02	0.02	0.3	0
26	-0.06	0.02	0.6	0.1
27	-0.04	0.02	0.6	0.1
29	-0.05	0.06	0.7	0.2
30	-0.02	0.03	0.5	0.2
31	-0.01	0.02	0.4	0.2
32	-0.01	0.02	0.6	0.4
33	-0.02	0.07	0.9	0.4
34	0.02	0.02	0.6	0.2
35	0.00	0.04	0.7	0.2
36	-0.03	0.02	0.7	0.2
37	-0.02	0.04	0.6	0.3

Table 7: Results of the averaged \overline{V}_e and \overline{U}_e calculated by using the elliptic fit model of the data of the stable regime. No.28 is not listed here, as its resulting iso-correlation contour plot doesn't fulfill the requirement of elliptic shaped iso-contour lines for the elliptic fit method, which leads to the impossibility of applying this method to their iso-correlation contour plots.

8 Discussion

To discuss the applicability of the elliptic model to the measured data sets we compare the results of the two applied methods with the measured data. The outcome will show whether the application of the elliptic model to the data is valid or not. I will first discuss the correlation between the measured velocities and the calculated velocities by the Maximum method respectively the Elliptic fit method. To do so, the measured mean velocity U_{meas} is plotted against U_m and \overline{U}_e and by analogy the measured sweeping velocity V_{meas} against V_m and \overline{V}_e . The outcome can be seen in 18 for the labile and in 19 for the stable regime. In both figures, the five nonfunctional data (No.1, No.3, No.4, No.5 and No.6) are left out due to the lack of calculations of the elliptic model. The omission is also further motivated in the following discussion.

A recognizable coincidence between two variables plotted against each other would be evident by the points forming an increasing line, which can't be observed in either of these eight plots. This leads to the conclusion that there is no correlation between the measured velocities and the calculated ones using the methods.

This uncorrelatedness is the result of various causes, which we will now look at individually.

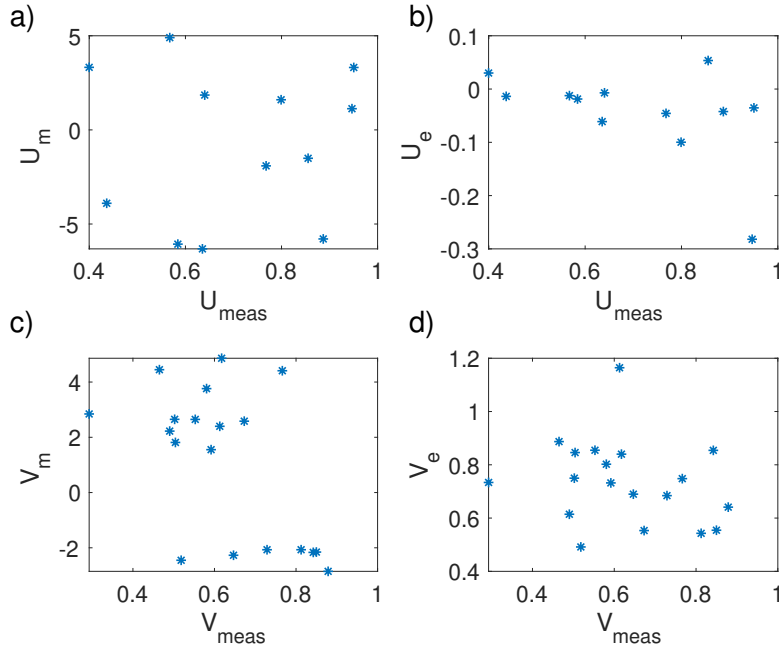


Figure 18: Correlation between U_{meas} and U_m respectively U_e and the correlation between V_{meas} and V_m respectively V_e of the labile regime

Significance of iso-correlation contour patterns Firstly we discuss the visual result of the iso-correlation contour plots as it can be a possible explanation for the uncorrelatedness between the calculated and measured velocities. In the beginning of the result section I displayed different types of iso-contour plots. The missing of elliptic lines in the iso-contour plots of figure 13 leads to the impossibility of applying the elliptic fit method, and also the application of the maxima fit method leads to unsatisfying results. Reason for this assumption are the high errors we can see in table 6 of V_m of No.3, No.4, No.6 and the error of U_m of No.1, leading to no meaningful results for the velocities U_m and V_e . In addition even though No.5 does not have a high error, one can see in figure ??(a) that the relation of r and τ_p is not linear increasing. A similar result can be seen in figure ??(b) for τ and r_p , as they are also not linear increasing. Therefore the applications of the maxima fit method with the equations (19) and (20) is not leading to informative results for U_m and V_m . This data set is an example to state that for some data sets there is a discrepancy of expectable values of U_m and V_m , but which are based on non linearly increasing scatter plot of r and τ , and therefore not results. Therefore apart from the results of U_m and V_m and their error

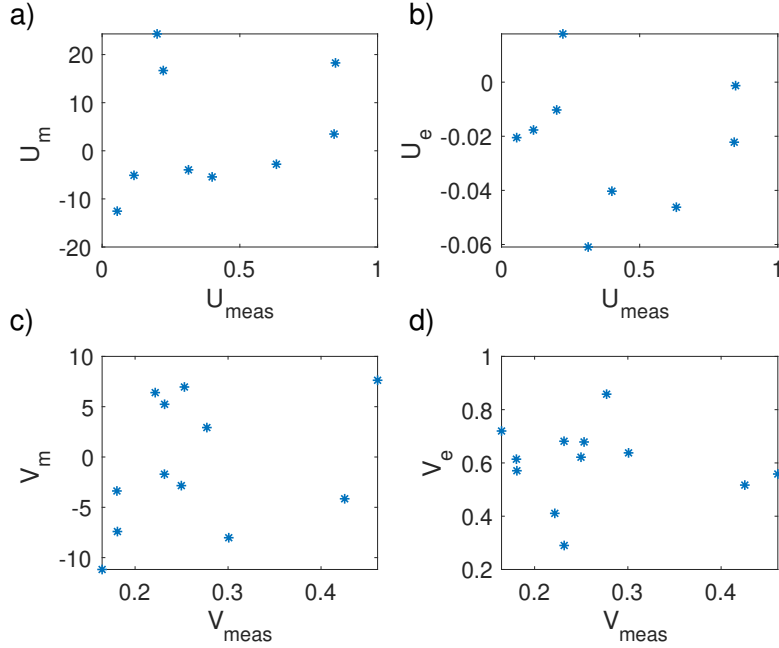


Figure 19: Correlation between U_{meas} and U_m respectively U_e and the correlation between V_{meas} and V_m respectively V_e of the stable regime

values, it is important to control the plotted figures.

In the figure 12(a) we can see a very sharp drop of the correlation value from $C_{TT}(r, \tau)=1$ to $C_{TT}(r, \tau)=0.3$ in less than $r = 0.25m$ respectively $\tau = 5s$. The data set displayed is No.8, but the phenomenon also applies to several other data. The application of the elliptic fit method to this data is possible, but the difference of correlation values between the value of the biggest enclosed iso-contour line and the value of the smallest enclosed line consisting of a minimum of 10 points is smaller than $\Delta C_{TT}(r, \tau) = 0.1$ on average. This short range leads to no representative velocity results for the data sets.

Another pattern of iso-correlation contour plots to be found, is a result of very slow decorrelation of the data and can be seen in figure 12(b) for the data set No.24. The analysis about the informative power of its results for U_e and V_e can leads to analogous conclusions as the analysis about the sharp decorrelation. The correlation value range for applicability of the elliptic fit method is very on average $\Delta C_{TT}(r, \tau) = 0.19$. The average of the calculated $V_e(C_{TT})$ and $U_e(C_{TT})$ is due to its short iso-contour value range also not leading to a representative outcome for the data set. This phenomenon also applies to the data of No.28 and No.32, and can be seen as extremely high errors of the mean velocity U_m in the table 5.

Significance of smoothness of iso-correlation contour lines The elliptic fit algorithm works on the minimization principle, which works better, the more elliptic shaped the iso-contour lines are. We can see in figure 11 that the iso-contour lines are elliptic shaped, but not really smooth, which affects the functionality of the fit algorithm. Therefore we can find the degree of smoothness strengthening the discrepancy of the measured and the calculated velocity values. The missing smoothness of the iso-contour lines of the measured correlation function can be a result of the complexity and uncontrollable atmospheric boundary conditions as it is discussed in the paper [6] by Han and Zhang. Reasons for the deviation of the standard form of an ellipse have been studied upon before and they came to the conclusion that the deviation can be attributed to the asymmetric shape of thermal plumes, and temperature fluctuations becoming inhomogeneous [26].

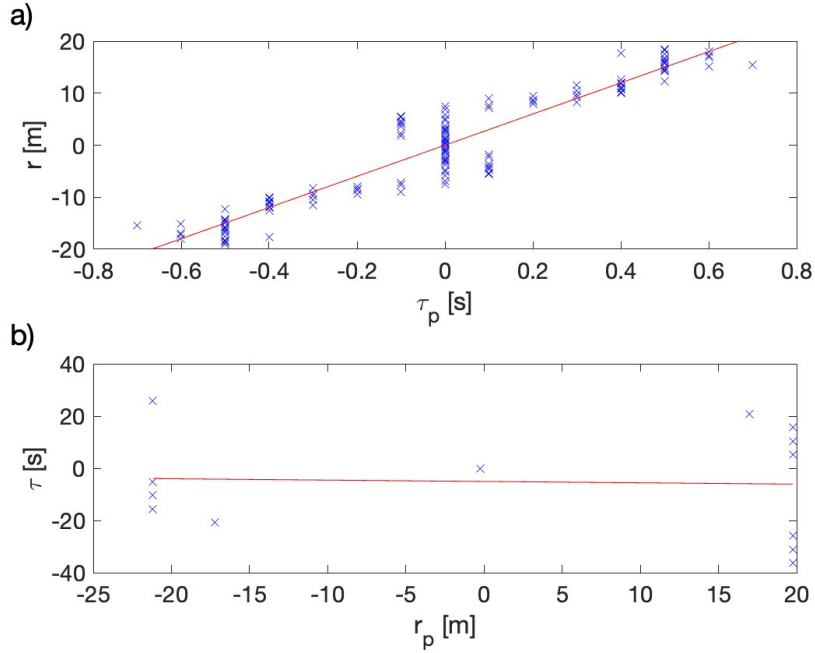


Figure 20: Result of the application of the maxima fit method to the data set No.5 in the labile regime. We can see the in a the a) Spatial shift r versus τ_p . The blue crosses represent each the temporal spacing τ_p which maximises the correlation function $C_{TT}(r, \tau)$ for specific values of streamwise spacing r . The red line is a linear fit to these data points. The fit is done with the prefabricated fit function `fitlm` in MatLab. The assumption of the dots increasing linearly is not fulfilled, as specific values of τ_p are connected to different values of r . b) Temporal shift τ versus r_p . The blue crosses represent each the temporal spacing r_p that maximises the correlation function $C_{TT}(r, \tau)$ for a specific τ . The assumption of the maxima fit method is a direct proportionality of τ and r_p , which is not fulfilled in this case, leading to no valid result for the gradient $C_U = 1/U_m$ and therefore not for U_m

Significance of averaging measured parameters over one hour An other topic of concern is the erroneous assumption of taking the value of U_{meas} as representative for the hourly situation. The averaging over one hour of measured data leads to an error of the value of U_{meas} and V_{meas} . The wind velocity is a very dynamical parameter that can change very quickly over a short period of time. Over such a period, the wind can vary its strength and therefore its velocity value and could also change its direction. Therefore its mean does not represent the real situation, but a mix of different occasions. Especially due to the restriction of the mean velocity to small velocity values of 1 m/s or less, the value of the mean velocity U_{meas} could be the result of averaging of stronger, but direction-changing-wind. Besides the mean velocity, all other measured parameters are also averaged over the one hour period. This could lead to the case that we mix different regimes, as the change of one regime to an other is not hourly restricted. Therefore it could happen, that different situations were merged together, resulting in one regime by averaging.

But there is evidence, that for the labile regime the measured and averaged wind direction over one hour is valid, because we can find a connection between the sign of U_m and the angle of the wind direction in the labile regime. As described in the section experimental set up, the wind that was measured with an angle range of 351° to 21° , represents a north wind and the wind measured with an angle range of 171° to 201° is a south wind. Despite these opposite directions of the wind, the measured mean velocity is positive in both cases. This is based on the implementation method of the velocity measurement, which only measures the absolute value of the velocity. But comparing the sign of the calculated mean velocity U_m and the angle of the wind leads to a direct coincident between the origin of south and north wind and the sign of U_m . We can therefore retract the winds origin out of the sign of U_m . The positive sign represents the south wind and the negative one the north wind. The three data (No.3, No.5, No.6) not supporting this conclusion are the data described as erroneous before.

This conclusion does not apply for the stable boundary layer as 8 of the 13 data sets result in the opposite conclusion. We can assume, that the origin of the wind for the conducted data in the labile regime is more stable over the period of an hour, compared to the conducted once in the stable regime.

Operability of the maxima fit method and the elliptic fit method Besides the shape of the iso-correlation contour plots, the operability of the maxima and the elliptic fit method have to be discussed. We can see in the table 6 that the value of the calculated mean velocity U_e is 19.2 times smaller than the measured U_{meas} in the labile regime and in table 7 that the factor is 14.5 times to the measured U_{meas} in the stable regime. Due to the independence of these factors to the above discussed iso-correlation contour patterns, we can conclude that it is based on the operability of the fitting algorithm. The reason for the mismatch is that the fitting algorithm of the elliptic fit is not able to find the right angle of the oblique ellipse, when fitting to the iso-correlation contour lines. This leads to erroneous values of the calculated mean velocity U_e and applies to the fitting to all correlation iso-contour plots. This error results in an average angle of approximately zero degree, which is directly proportional to the value of mean velocity and therefore U_e is approximately zero. We can conclude that the results of the elliptic fit method is therefore much better for smaller U , as the iso-contour lines then represent ellipses which are not rotated. The error of the elliptic fit method leading to this limitation could be fixed by implementing a better elliptic fit algorithm that is able to adjust to the angle more precisely.

When we analyse the outcome of the maxima fit method in the figures 14(b) and 15(b), we can see that there are only 12 points available for the fitting. This leads to a high uncertainty for the gradient C_U and with its direct relation of $C_U = 1/U_m$ to a high uncertainty for the mean velocity U_m . The reason for the low data point availability is the low temporal resolution of $\Delta\tau = 5.2\text{s}$.

We can see by comparing the tables 2 to 7 that the magnitudes of the measured sweeping velocity V_{meas} and the calculated V_m and V_e match. In addition the magnitudes of the measured mean velocity U_{meas} and the calculated mean velocity U_m using the maxima fit method match. Therefore we can conclude that besides the before discussed uncorrelatedness between the measured velocities and the calculated velocities, we can conclude that the application and usage of the maxima fit method and the elliptic fit methods to the measured data is valid and is leading to reasonable results.

The last topic to discuss about my results before I summarize suggestion for improvement, is the comparison of the results of the labile regime with those of the stable regime. There was no significant difference between the results of the data sets of the labile regime and the results of the stable regime. I can therefore conclude, that the separation is important for the averaging done with the wavelet function, but does not show in the results. With a higher spatio and temporal resolution of further studies that could differ and should therefore considered to be subject of further studies.

Suggestions for improvement for further studies Future studies should take into account that the accuracy of the mean velocity U is correlated with the temporal spacing. Therefore we can conclude that higher temporal resolved data have a direct impact on the results. In addition it is very important to have a bigger spatial field set-up. This is important as the ellipse method has its lower limit at the correlation value of which its iso-contour line was still enclosed. A bigger range of the spatial shift r would lead to a bigger range of enclosed iso-contour lines to which an ellipse can be plotted to. As described in the method section, I averaged spatially with a different number of samples for different spatial shift values r . This was necessary for conducting a spatial normalisation without losing correlation data along the spatial shift direction. But this lead to a distorted results as we only have one value for the spatial shift $r = \pm 40\text{m}$. Therefore a bigger viewing field for conducting data would lead to a more valid averaging. Furthermore, the limited conducting area can influence the shape of the iso-correlation contour lines due to the resulting incomplete convergence as it is discussed in the paper [27] by Metzger. In addition the spatial resolution should be considered to be conducted higher in further studies, as it would lead to smoother iso-contour lines. As we discussed earlier, the smoothness is a factor for the operability of the elliptic fit method and therefore we would achieve better results for the velocity calculations.

9 Conclusion

The analysis of the space-temporal-correlation in the atmospheric boundary layer has shown how the elliptic model can be applied using the maxima fit and the elliptic fit method.

The results of the calculated sweeping velocities V show the same magnitude as the measured one, and the maxima fit method also results in the same scales for the mean velocity U as the measured one. This leads to the conclusion that the mean velocity and sweeping velocity can be calculated out of the temperature fluctuating data, conducted of the field experiment by applying the elliptic model.

But apart from the scaling, the values of the calculated velocities differ a lot from the measured ones leading to a high uncorrelatedness between the calculated and the measured velocity values. These results can be based on iso-correlation contour patterns of the correlation functions, which is the result of three different reasons. The first one is the resolution of the spatial and temporal data, the second is the complexity and uncontrollability of the atmospheric boundary condition and the third is due to the averaging over one hour leading to errors introduced by averaging different atmospheric boundary flows. The latter one leads to erroneous values for the measured mean velocity U_{meas} , sweeping velocity V_{meas} , and the spatial-temporal correlation, which can therefore not be used for a valid comparison between the calculated velocities with the maxima fit method and the elliptic fit method.

The comparison of my results of the spatio-temporal correlation and the calculated mean and sweeping velocities with the results of the paper [6] by Han and Zhang lead to the conclusion, that spatial and temporal resolution are directly related with the accuracy of the results. Therefore it is important to review the analysis with data conducted with higher spatial and temporal dissolution and a broader spatial range to further validate the elliptic model applied to atmospheric boundary flow.

References

- [1] Guo-Wei He and Jin-Bai Zhang. “Elliptic model for space-time correlations in turbulent shear flows”. In: *Physical Review E* 73.5 (2006), p. 055303.
- [2] Richard Davy. “The climatology of the atmospheric boundary layer in contemporary global climate models”. In: *Journal of Climate* 31.22 (2018), pp. 9151–9173.
- [3] Robert A Brown. *Fluid mechanics of the atmosphere*. Academic Press, 1991.
- [4] Karthik Duraisamy, Gianluca Iaccarino, and Heng Xiao. “Turbulence modeling in the age of data”. In: *Annual review of fluid mechanics* 51 (2019), pp. 357–377.
- [5] Ideen Sadrehaghighi. “Turbulence Modeling”. In: *A Review, Report* 1.86 (2019), p. 9.
- [6] GuoWen Han and XiaoBin Zhang. “A Predictive Method for Estimating Space–Time Correlations in the Atmospheric Surface Layer”. In: *Boundary-Layer Meteorology* 184.3 (2022), pp. 423–440.
- [7] Christoph K Thomas et al. “High-resolution fibre-optic temperature sensing: A new tool to study the two-dimensional structure of atmospheric surface-layer flow”. In: *Boundary-layer meteorology* 142 (2012), pp. 177–192.
- [8] John Roy Garratt. “Review: the atmospheric boundary layer”. In: *Earth-Sci. Rev* 37.1 (1994), pp. 89–134.
- [9] Geoffrey Ingram Taylor. “The spectrum of turbulence”. In: *Proceedings of the Royal Society of London. Series A-Mathematical and Physical Sciences* 164.919 (1938), pp. 476–490.
- [10] Uriel Frisch. *Turbulence: the legacy of AN Kolmogorov*. Cambridge university press, 1995.
- [11] Gabriel Katul et al. “The random sweeping decorrelation hypothesis in stratified turbulent flows”. In: *Fluid dynamics research* 16.5 (1995), pp. 275–295.
- [12] MJ Fisher and POAL Davies. “Correlation measurements in a non-frozen pattern of turbulence”. In: *Journal of fluid mechanics* 18.1 (1964), pp. 97–116.
- [13] Yu Cheng et al. “Failure of Taylor’s hypothesis in the atmospheric surface layer and its correction for eddy-covariance measurements”. In: *Geophysical Research Letters* 44.9 (2017), pp. 4287–4295.
- [14] A Bahraminasab et al. “Taylor’s frozen-flow hypothesis in Burgers turbulence”. In: *Physical Review E* 77.6 (2008), p. 065302.
- [15] KA Everard et al. “Sweeping effects modify Taylor’s frozen turbulence hypothesis for scalars in the roughness sublayer”. In: *Geophysical Research Letters* 48.22 (2021), e2021GL093746.
- [16] Xiaozhou He and Penger Tong. “Space-time correlations in turbulent Rayleigh–Bénard convection”. In: *Acta Mechanica Sinica* 30 (2014), pp. 457–467.
- [17] Peng-Jun-Yi Zhang, Zhen-Hua Wan, and De-Jun Sun. “Space-time correlations of velocity in a Mach 0.9 turbulent round jet”. In: *Physics of Fluids* 31.11 (2019).
- [18] Wei Wang, Xin-Lei Guan, and Nan Jiang. “TRPIV investigation of space-time correlation in turbulent flows over flat and wavy walls”. In: *Acta Mechanica Sinica* 30.4 (2014), pp. 468–479.
- [19] Michael Wilczek and Yasuhito Narita. “Wave-number–frequency spectrum for turbulence from a random sweeping hypothesis with mean flow”. In: *Physical Review E* 86.6 (2012), p. 066308.
- [20] C.K. Thomas and J.S. Selker. “Optical fiber-based distributed sensing methods”. In: *Springer Handbook of Atmospheric Measurements*. Ed. by Th. Foken. Springer Handbooks, Springer Nature Switzerland AG 2021, 2021. Chap. Chapter 20, pp. 609–631.
- [21] Matthias J Zeeman, John S Selker, and Christoph K Thomas. “Near-surface motion in the nocturnal, stable boundary layer observed with fibre-optic distributed temperature sensing”. In: *Boundary-layer meteorology* 154 (2015), pp. 189–205.
- [22] Dan Li and Elie Bou-Zeid. “Coherent structures and the dissimilarity of turbulent transport of momentum and scalars in the unstable atmospheric surface layer”. In: *Boundary-Layer Meteorology* 140 (2011), pp. 243–262.

- [23] Christopher Torrence and Gilbert P Compo. “A practical guide to wavelet analysis”. In: *Bulletin of the American Meteorological society* 79.1 (1998), pp. 61–78.
- [24] Marie Farge. “Wavelet transforms and their applications to turbulence”. In: *Annual review of fluid mechanics* 24.1 (1992), pp. 395–458.
- [25] Chr Thomas and Th Foken. “Detection of long-term coherent exchange over spruce forest using wavelet analysis”. In: *Theoretical and Applied Climatology* 80 (2005), pp. 91–104.
- [26] Xiaozhou He and Penger Tong. “Kraichnan’s random sweeping hypothesis in homogeneous turbulent convection”. In: *Physical Review E* 83.3 (2011), p. 037302.
- [27] M Metzger, BJ McKeon, and H Holmes. “The near-neutral atmospheric surface layer: turbulence and non-stationarity”. In: *Philosophical Transactions of the Royal Society A: Mathematical, Physical and Engineering Sciences* 365.1852 (2007), pp. 859–876.

Selbstständigkeitserklärung

Die Verfasserin erklärt, dass sie die vorliegende Arbeit selbständig, ohne fremde Hilfe und ohne Benutzung anderer, als der angegebenen Hilfsmittel angefertigt hat. Die aus fremden Quellen (einschließlich elektronischer Quellen) direkt oder indirekt übernommenen Gedanken sind ausnahmslos als solche kenntlich gemacht. Die Arbeit ist in gleicher oder ähnlicher Form oder auszugsweise im Rahmen einer anderen Prüfung nicht vorgelegt worden.

A handwritten signature in black ink, reading 'Charlotte Geiger'. The signature is written in a cursive style with a large, looping 'G' at the end.

Charlotte Geiger, Bayreuth, den 12.10.2023